

## CHAPTER V

Probing hydrogen bond potentials via combination band spectroscopy: a near IR study of the geared bend/van der Waals stretch intermolecular modes in (HF)<sub>2</sub>

### 5.1 Introduction

The hydrogen bond is of pivotal importance in many areas of science and has stimulated enormous efforts directed toward elucidating its fundamental properties. One approach that continues to provide quantitative information on hydrogen bond interactions is the study of small hydrogen bonded clusters via high resolution molecular spectroscopy.<sup>1-6</sup> Due to the presence of large amplitude *intermolecular* motion of the constituent monomers within the complex, the spectra of these hydrogen bonded clusters can be qualitatively different from those of covalently bonded species, demonstrating effects due to frustrated internal rotation, tunneling, predissociation, etc. Indeed, spectroscopic data on this large amplitude motion provide important constraints on the strength and angular anisotropy of the hydrogen bond potential energy surface (PES). As a necessary parallel thrust, theoretical quantum mechanical (QM) methods have made major advances recently which now allow "exact" solution of the Schrödinger equation for nuclear motion in 4 atom hydrogen bonded dimers such as HX-HY (X, Y = Cl, F). Thus, these clusters offer particular advantages for rigorous study of the hydrogen bond surface: large amplitude nuclear motion of the light hydrogenic

masses samples the potential in considerable detail, and yet the clusters are sufficiently small to facilitate both experimental and theoretical investigation with full quantum state resolution.

One system which has long been at the focus of combined high-level theoretical and experimental scrutiny is the hydrogen fluoride dimer [(HF)<sub>2</sub>] and its isotopomers. Though the simplest 4 atom prototype of a hydrogen bond, HF dimer displays a remarkable diversity of dynamical behavior, which has been extensively investigated by high-resolution studies in the microwave,<sup>7-10</sup> far-IR,<sup>11-14</sup> and near-IR.<sup>15-21</sup> As a consequence of such efforts, accurate data are now available for the dissociation energy, tunneling splittings, and predissociation lifetimes, with particular experimental emphasis on the high frequency, *intramolecular* degrees of freedom. Analytical representations of the full  $3N-6 = 6$  potential have been presented by Hancock *et al.*<sup>22</sup> and Bunker *et al.*<sup>23</sup> based upon fits to high level *ab initio* calculations. Of particular relevance to this paper is the analytical potential surface (SQSBDE) by Quack and Suhm,<sup>24</sup> which was fitted to the points of Karpfen *et al.*,<sup>25</sup> but also empirically modified to reflect the microwave, far- and near-IR spectroscopic and bond dissociation data<sup>4,26</sup> available at that time. Indeed, this potential has served as a benchmark surface for full quantum calculations in numerous contexts<sup>27-38</sup> and has proven reasonably consistent with much of the experimental results. As will be demonstrated herein, the SQSBDE potential does a reasonably good job at reproducing spectroscopic properties of the intermolecular vibrations; however, there are significant discrepancies that this study also reveals.

High resolution vibration-rotation-tunneling (VRT) spectroscopy of weakly bound clusters, especially associated with intermolecular excitation, is a powerful method for extracting information on the attractive part of intermolecular potentials. In HF dimer, the two intramolecular (i.e., "covalent") vibrational modes correspond to excitation of the hydrogen acceptor ( $\nu_1$ ) and the hydrogen donor ( $\nu_2$ ) subunits, and absorb in the near-IR region close to the free HF monomer stretch around  $4000\text{ cm}^{-1}$ . The four intermolecular (i.e., "hydrogen bonded") modes reflect large amplitude nuclear motion of the two HF moieties, and occur in the far-IR region between  $100$  and  $500\text{ cm}^{-1}$ . Due to the existence of a double minimum on the  $(\text{HF})_2$  potential energy surface separated by a relatively low barrier ( $\sim 350\text{ cm}^{-1}$ ), the intermolecular modes are characterized by strongly coupled and highly anharmonic dynamics that are better described as tunneling motions or hindered internal rotations. These four intermolecular vibrational modes correspond approximately to an "anti-gear bend" ( $\nu_3$ ), a "van der Waals stretch" ( $\nu_4$ ), a "gear bend" ( $\nu_5$ ), and an "out-of-plane torsion" ( $\nu_6$ ) motion of the HF diatoms, though due to coupling in the potential surface or near resonances, there may be substantial blurring of these zero order descriptions. Despite the considerable experimental attention HF dimer has received, the majority of spectroscopic data reflect either the vibrational ground state, or excitation of the high frequency intramolecular modes. There have been several far-IR studies by Quack and coworkers<sup>12-14</sup> using static cooled cells. However, a combination of resolution, pressure broadening and considerable spectral congestion at these relatively high cell temperatures and pressures renders the spectral analysis

difficult. There has also been a near-IR study of a few combination bands by Miller and coworkers<sup>21</sup> to which we will make comparison. These are taken under low temperature, high resolution molecular beam conditions, but also with lower detection sensitivity than currently demonstrated with the slit jet spectrometer. Thus, although the available potential surfaces appear to reproduce many of the previous experimentally observed quantities, high resolution jet studies of all four intermolecular vibrational degrees of freedom in (HF)<sub>2</sub> are still necessary to provide a far more demanding and rigorous set of tests.

Of direct relevance to the present studies, both the intra- and intermolecular dependence of the HF dimer PES can be simultaneously probed in the near-IR via combination bands of the intermolecular modes built on one quantum of intramolecular HF stretch. To the extent that the upper states can be characterized by the full 3N-6 potential surface adiabatically averaged over intramolecular excitation, such near-IR studies form the perfect compliment to previous work from the far-IR and microwave studies, which sample the intermolecular potential surface adiabatically averaged over the intramolecular *ground* state. However, this adiabatic treatment is necessarily approximate, which therefore also permits qualitatively new dynamics in the *excited* intramolecular states to be investigated, such as state-resolved predissociation, coupling of the intra/intermolecular degrees of freedom, vibrationally inhibited tunneling, etc.<sup>15,17,18,20,39</sup> Thus, the present near-IR studies both synergistically build on previous and ongoing studies in the far-IR/microwave regions, and yet exploit

advantages posed by tunable near-IR laser methods to probe dynamical phenomena not accessed with lower frequency spectral probes.

This near-IR access to low-frequency intermolecular modes comes at a significant cost: the combination bands are generally much weaker (by  $10^1$ - $10^3$  fold) than the intramolecular fundamentals. Fortunately, the high sensitivity ( $10^7$ - $10^8$  molecules/cm<sup>3</sup>/quantum state) of the current difference frequency spectrometer and the low temperature/long absorption path environment of the slit supersonic expansion is sufficient to monitor the HF dimer intramolecular fundamentals with signal to noise in excess of 2000:1. Depending on the degree of spectral broadening from vibrational predissociation, this direct absorption method therefore permits weak combination bands down by as much as 3 orders of magnitude from the fundamental bands to be observed over continuously tunable regions of the infrared.

An important advantage of studying intermolecular modes via intra/intermolecular combination bands is the relatively broad access that tunable near-IR lasers offer over wide spectral regions. For example, continuous high resolution spectral scans over several hundreds of cm<sup>-1</sup>s at  $\leq 0.001$  cm<sup>-1</sup> resolution are more or less "routine", which greatly facilitates a systematic search for a specific combination band. Furthermore, the intensity information obtained from such near-IR direct absorption methods is experimentally quite reliable and can be tested against predictions from full quantum calculations. As will be shown below, the observed oscillator strengths can vary dramatically from one combination band to another, and thereby provides an additional mode specific

probe of the coupling between inter and intramolecular excitation. Indeed, in conjunction with continuous coverage over a given spectral region, even the absence of a given band is often informative, and establishes rigorous lower limits on its experimental oscillator strength. Stated generally, intensity information represents a specific example of a general class of spectroscopic probes more sensitive to the *eigenfunction* than simply just the *eigenvalue*. In conjunction with full multidimensional QM calculations, these data provide an important new source of quantitative information for testing intermolecular potentials from experiment.

Reported herein is the first of two chapters on high resolution combination band spectroscopy and dynamics of HF dimer. In this first chapter, combination bands in the region between 3900 and 4150  $\text{cm}^{-1}$  associated with the two lowest energy intermolecular modes, the  $\nu_4$  "van der Waals stretch" and  $\nu_5$  "geared bend", will be discussed. In chapter VI, spectra and analysis of the two remaining modes,  $\nu_3$  "anti-geared bend" and  $\nu_6$  "out-of-plane torsion" will be presented. The analysis of these rotationally resolved spectra yields accurate spectroscopic constants, intermolecular energies, and tunneling splittings for all four states that include quanta of both intra- and intermolecular vibrational excitation. The two intermolecular modes discussed herein correspond classically to motion along the tunneling and radial van der Waals stretching coordinates, thus providing information on the topology of the PES particularly near the barrier to donor-acceptor interchange. In addition, predissociation broadening in the combination band spectra is observed to be strongly mode specific. This behavior is similar to

the  $\nu_1$  versus  $\nu_2$  predissociation rates first observed in the intramolecular fundamentals, but with systematic sensitivity to further intermolecular excitation. Finally, comparison of the new spectroscopic data with recent QM calculations of the VRT energy levels allow trial potential energy surfaces to be quantitatively evaluated.

## 5.2 Experimental

The experimental technique employed is essentially identical to that used for previous studies,<sup>40,41</sup> with minor modifications for optimum generation of (HF)<sub>2</sub>. Details of the apparatus are presented in Chapter 2 and will only succinctly be reviewed here. Briefly, the spectra of (HF)<sub>2</sub> combination bands are recorded in a slit supersonic jet using direct absorption IR methods based on a tunable difference frequency laser spectrometer. Narrow band ( $\leq 1$  MHz) infrared light is produced via cw non-linear difference frequency mixing of visible, single mode Ar<sup>+</sup> (488.0 nm) and dye (R6G) lasers in a temperature controlled LiNbO<sub>3</sub> crystal.<sup>42</sup> The infrared light thus generated is split into a reference and a signal beam, with the IR power on the reference beam monitored with a photovoltaic, liquid N<sub>2</sub> cooled InSb detector. The IR power on the signal beam is monitored on a matched InSb detector, after multipassing 20 times through the long axis of a pulsed, slit jet (4 cm  $\times$  190 *mm*) supersonic expansion. The IR power of the signal beam is subtracted from the reference power, thereby eliminating common mode noise due to Ar<sup>+</sup> and dye laser fluctuations. Differences arising from signal

beam absorption within the duration of the expansion pulse are recorded as a function of IR laser frequency. The relative infrared frequencies are determined by monitoring dye laser transmission fringes through a stabilized Fabry-Perot optical transfer cavity,<sup>40,41</sup> to which the Ar<sup>+</sup> laser is servo loop locked as well. This technique permits measurement of relative frequencies to better than 0.0001 cm<sup>-1</sup>, as verified by routine agreement with microwave ground state combination differences at the 3-5 MHz level. Absolute frequency calibration is achieved by referencing to the R(0), R(2), and R(3) lines of monomeric HF at 4000.9894, 4075.2936, and 4109.9363 cm<sup>-1</sup>, respectively.<sup>43</sup> This calibration procedure allows the transition frequencies and vibrational origins to be reported to an absolute accuracy of 0.0002 cm<sup>-1</sup>.

The (HF)<sub>2</sub> complex is formed by adiabatically expanding mixtures of 1.0% HF in a He/Ne/Ar buffer gas mixture at a backing pressure of 450 Torr, resulting in rotational temperatures of 8-10 K. The buffer gas composition found to optimize the formation of (HF)<sub>2</sub> is a 50:50 mixture of Ar and "first-run" Ne (70% Ne, 30% He). Absorbances in excess of 5% are typically observed (S/N > 2000) for the strong  $\nu_1 K_a = 1 \leftarrow 0$  fundamental, corresponding to concentrations at 1 cm downstream from the slit nozzle of  $3 \times 10^{10}$  (HF)<sub>2</sub> molecules/cm<sup>3</sup>. As first noted in previous studies,<sup>44</sup> small amounts ( $\leq 2\%$ ) of N<sub>2</sub>O in the mixture promote the formation of (HF)<sub>2</sub> in the jet, ostensibly via formation of the more weakly bound HF-N<sub>2</sub>O complex that is "displaced" by a subsequent collision with HF. Therefore, in spectral searches for the weaker combination bands the samples have been purposely doped with trace amounts of N<sub>2</sub>O. This leads to occasional

extremely weak, multiple quantum overtone and combination band N<sub>2</sub>O monomer transitions observed in the region scanned. However, these bands are well known<sup>45</sup> and at sub-Doppler 0.001 cm<sup>-1</sup> resolution, any such N<sub>2</sub>O signals are readily distinguished from the characteristic and widely spaced spectral pattern due to (HF)<sub>2</sub>.

### 5.3 Results and analysis

#### 5.3.1 Background

As known from early microwave studies,<sup>7</sup> the potential surface for HF dimer has two equivalent wells which support a large amplitude tunneling motion that interchanges the role of hydrogen bond donor and acceptor HF subunits. Consistent with such large amplitude motion on a floppy potential surface, the overall symmetry of each HF dimer VRT energy level is best analyzed using permutation-inversion (PI) group theory,<sup>46-50</sup> specifically the M<sub>S4</sub> molecular symmetry group. In this PI group, A/B refer to symmetry/antisymmetry with respect to simultaneous interchange of both H and F nuclei, whereas the +/- refer to the total parity, i.e., inversion of all nuclei through the origin.

For purposes of correctly assigning the observed HF dimer combination bands, it is advantageous to break this rigorous VRT symmetry down further into a product of the tunneling ( $\Gamma_{\text{tun}}$ ), vibrational ( $\Gamma_{\text{vib}}$ ), and rotational ( $\Gamma_{\text{rot}}$ ) symmetries

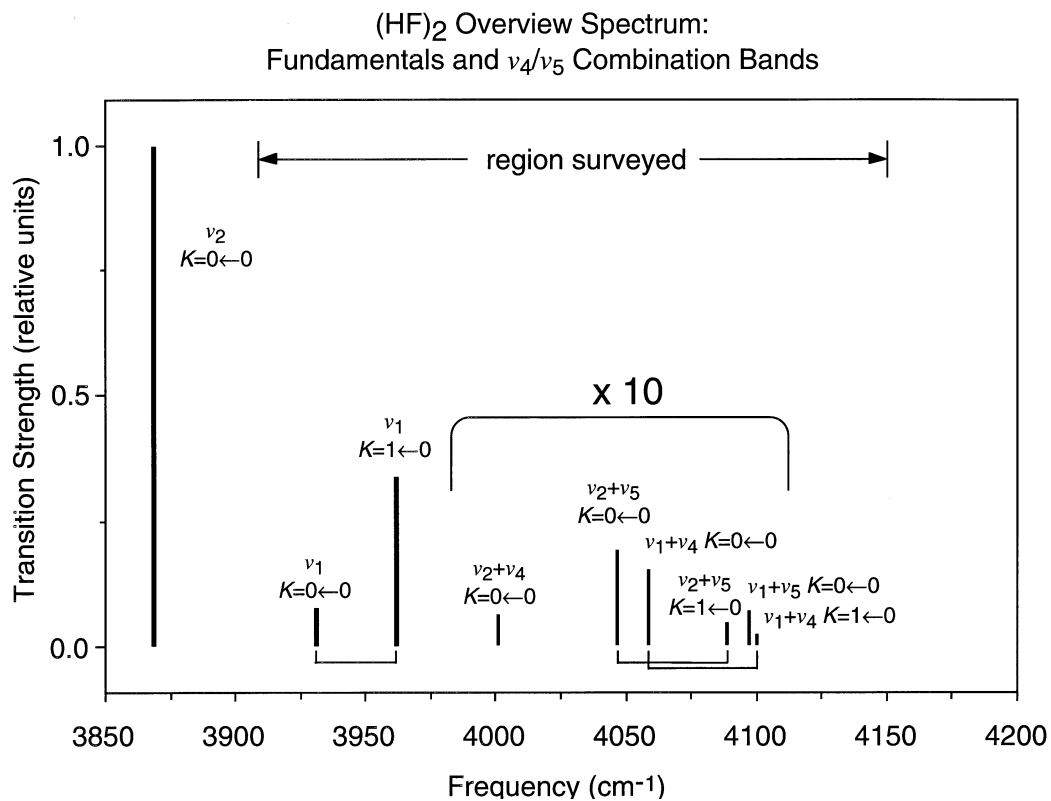


Figure 5.1 Overview of the HF dimer spectrum between 3850 and 4200  $\text{cm}^{-1}$  with the region surveyed for combination bands indicated. Both the intramolecular HF stretching fundamentals and the  $\nu_4/\nu_5$  combination bands magnified ten times. For simplicity, only the origin of one tunneling component is shown for each combination band and fundamental.

with  $\Gamma_{\text{vrt}} = \Gamma_{\text{vib}} \otimes \Gamma_{\text{rot}} \otimes \Gamma_{\text{tun}}$ . Unlike total symmetry, these individual labels are approximate, but still meaningful in the limit of weak coupling between overall rotation, tunneling and the intermolecular vibrational degrees of freedom. More commonly, the experimentally observed bands are labeled by the  $\Gamma_{\text{vib-tun}}$  symmetry, with the rotational symmetry already factored out. If one takes electric dipole selection rules and conservation of nuclear spin symmetry into account, allowed vib-tun transitions are predicted between  $\Gamma_{\text{vib-tun}} = A^+ \leftrightarrow B^+$  and  $\Gamma_{\text{vib-tun}} = A^+ \leftrightarrow A^-, B^+ \leftrightarrow B^-$  symmetry states for in-plane ( $\Gamma_{\text{vib}} = A^+, B^+$ ) and out-of-plane ( $\Gamma_{\text{vib}} = A^-, B^-$ ) vibrations, respectively.

The tunneling splitting in a given vibrational state is defined<sup>51</sup> as the signed difference in the vibrational origins for the pair of tunneling states, i.e.,

$$\Delta\nu_{\text{tun}} = \nu_K(\Gamma_{\text{tun}} = B^+) - \nu_K(\Gamma_{\text{tun}} = A^+) \quad (5.1)$$

Only the product  $\Gamma_{\text{vib-tun}} = \Gamma_{\text{vib}} \otimes \Gamma_{\text{tun}}$  can be inferred directly from the spectra, therefore, the *sign* of the tunneling splitting remains undefined unless  $\Gamma_{\text{vib}}$  is somehow specified. The presence of strong anharmonic and/or Coriolis resonances that mix rotation, vibration and tunneling degrees of freedom, can in principle shift one level with respect to the other, and thereby change the sign of the tunneling splitting. However, in the absence of such strong near resonant state mixing, the state within a given tunneling pair which has an additional node along the tunneling coordinate ( $\Gamma_{\text{tun}} = B^+$ ), should be higher in energy than the nodeless

( $\Gamma_{\text{tun}} = A^+$ ) state. As defined by Eq. (5.1), this is equivalent to a prediction of a *positive* tunneling splitting for all inter and intramolecular vibrational states.

Thus, the energetic ordering of the total vib-tun symmetries ( $\Gamma_{\text{vib-tun}}$ ) for tunneling pairs can be used to infer the vibrational symmetry ( $\Gamma_{\text{vib}}$ ) of that state.

Similarly, for sufficiently weak coupling between inter/intramolecular degrees of freedom, the combination state vibrational symmetry can also be approximately factored into the corresponding product of the intra- and intermolecular vibrational symmetries, i.e.,  $\Gamma_{\text{vib}} = \Gamma_{\text{intra}} \otimes \Gamma_{\text{inter}}$ . Since the intramolecular vibrational frequencies are at least an order of magnitude greater than the corresponding intermolecular frequencies, an adiabatic separation of these degrees of freedom is anticipated to be well justified. The vibrational symmetries of the  $\nu_1$  and  $\nu_2$  intramolecular modes have been assigned by Mills<sup>50</sup> to  $\Gamma_{\text{intra}} = B^+$  and  $A^+$ , respectively. Both intermolecular modes (nominally the "van der Waals stretch" and "geared bend") described in this paper, are in-plane vibrations with  $\Gamma_{\text{inter}} = A^+$  symmetry. Thus, the overall vibrational symmetry ( $\Gamma_{\text{vib}}$ ) is dictated by the intramolecular vibrational symmetry (i.e.,  $\Gamma_{\text{vib}} = \Gamma_{\text{intra}} \otimes A^+ = \Gamma_{\text{intra}}$ ).

Consistent with the established convention<sup>17,18</sup> for (HF)<sub>2</sub>, term values for each tunneling and  $K=K_a$  state are fit separately using the expression,

$$E_K(J) = v_K + [\bar{B}_K \pm 1/2 b_K \delta_{K1}]J(J+1) - D_K J^2(J+1)^2 + H_K J^3(J+1)^3. \quad (5.2)$$

In Eq. (5.2)  $\nu_K$  is the energy of the  $J = 0$  (extrapolated for  $K > 0$ ) state for a given  $K$  level with respect to the  $J = 0, \Gamma_{\text{VRT}} = A^+ K = 0$  state of  $(\text{HF})_2$ . Furthermore,  $\bar{B}_K = (B_K + C_K)/2$ ,  $D_K$  and  $H_K$  are the  $K$ -dependent effective rotational and distortion constants in symmetric top notation, while the Kronecker delta  $\delta_{K1}$  brings in an asymmetry splitting term due to  $b_K = (B_K - C_K)/2$  which is only significant for  $K = 1$  levels. For all the spectra presented in this paper, the  $J$  and tunneling state labeling is unambiguously confirmed by well-determined ground state combination differences.<sup>8</sup> Thus, the ground state constants in the least squares fits are fixed at values determined from global fits to previous microwave and near-IR studies.<sup>14,52</sup> The sextic centrifugal distortion constant  $H_K$  is set to zero in the upper state due to the lack of sufficiently high  $J$  transitions necessary to determine this constant accurately.

Based on previous experimental data<sup>21,53</sup> and predictions of the intermolecular mode frequencies,<sup>36</sup> the search for HF dimer combination bands associated with the two lowest frequency intermolecular modes ( $\nu_4$  and  $\nu_5$ ) covers the  $250 \text{ cm}^{-1}$  region between  $3900$  and  $4150 \text{ cm}^{-1}$ . This search reveals 10 VRT bands, 6 previously unobserved, which reflect excitation in each of the  $\nu_4$  and  $\nu_5$  intermolecular modes, built on either the  $\nu_1$  or  $\nu_2$  intramolecular fundamentals. A stick spectrum which schematically summarizes the origin frequencies and relative integrated intensities for all the combination bands reported in this paper is shown in Figure 5.1. Note that even the strongest combination band is still 50-fold weaker than the corresponding parent fundamental and that an additional 10-

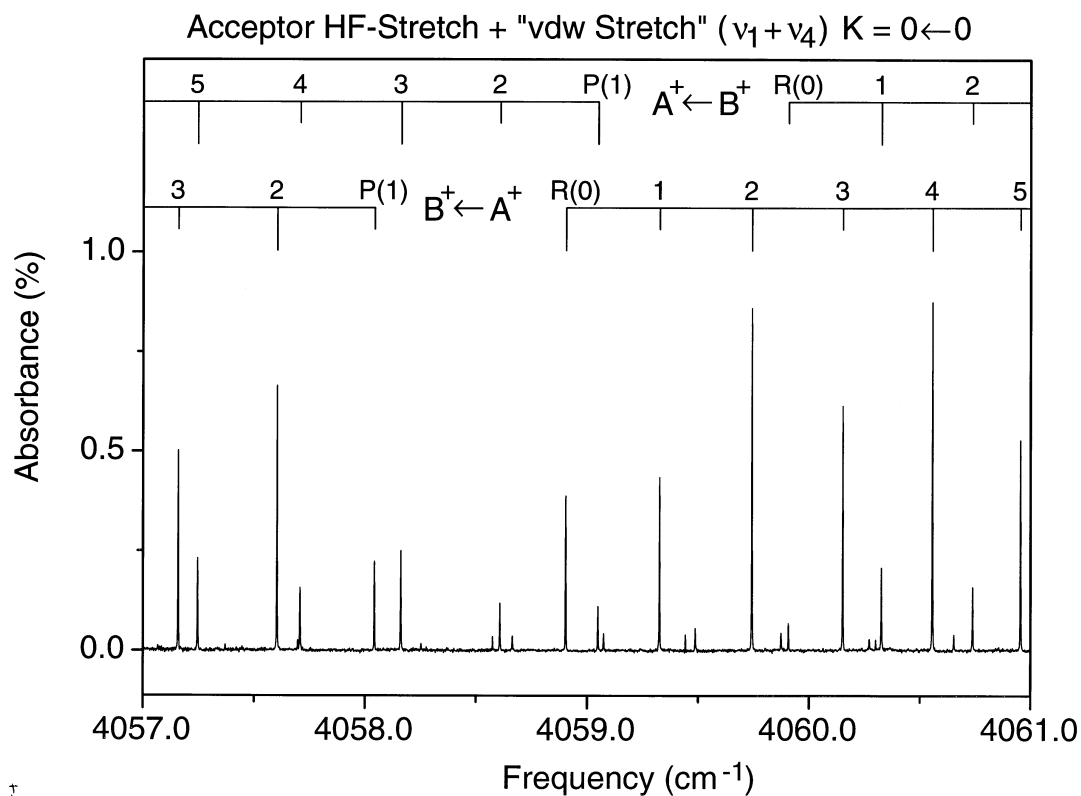
to 20-fold dynamic range exists in integrated intensities between the most intense ( $\nu_2+\nu_5$ ,  $K = 0\leftarrow 0$ ) and least intense ( $\nu_1+\nu_4$ ,  $K = 1\leftarrow 0$ ) combination bands.

Before we turn to analysis of the combination band spectra in detail, one point is worth noting. Since all the in-plane intermolecular vibrations are of the same  $\Gamma_{\text{vib}} = A^+$  symmetry, there can be strong mixing between these modes which can make a zero order description of the motion difficult and potentially misleading. This is especially likely for the "van der Waals stretch" and "geared bend" modes, which are close in energy and therefore susceptible to mixing by angular-radial coupling in the potential surface. Hence, the descriptive labels for these two vibrations will be left in quotations to remind us of their potentially approximate nature yet at the same time maintain continuity with previous studies.<sup>12,14,21</sup> (Conversely, the standard  $\nu_4$ ,  $\nu_5$  notation requires no such assumptions and provides a rigorously "correct" label, though of course with no physical insight!) Indeed, as will be elucidated below, the combination band rotational constants, predissociation lifetimes, and tunneling splittings in this work provide strong evidence for significant mixing between these "van der Waals stretch" and "geared bend" degrees of freedom. The appropriate zero order description of the low frequency intermolecular modes highlights an important discrepancy between experiment and theoretical predictions based on HF dimer potential surfaces, an issue which will be addressed in the discussion section.

### 5.3.2 $\nu_4$ ("van der Waals stretch")

#### 5.3.2a ( $\nu_1 + \nu_4$ ) $K = 0 \rightarrow 0$

The lowest frequency intermolecular mode ( $\nu_4$ ) in  $(\text{HF})_2$  is predicted from the 6D QM calculations<sup>28</sup> to be predominantly a "van der Waals stretch" motion at  $126.37 \text{ cm}^{-1}$ . In the limit of small off diagonal anharmonicity, one therefore anticipates the  $\nu_1 + \nu_4$  combination band to be near  $3931 + 126 = 4057 \text{ cm}^{-1}$ . Figure 5.2 shows a segment of the infrared spectrum in the vicinity of  $4059 \text{ cm}^{-1}$  where, in good agreement with this prediction, a pair of overlapping VRT bands are detected. There are two rotational progressions due to the tunneling motion in HF dimer, and both exhibit the intensity alternation characteristic of HF dimer spectra. The bands are moderately strong (although only  $\sim 4\%$  of the transition strength of the  $K = 1 \leftarrow 0$   $\nu_1$  fundamental) and the presence of both R(0) and P(1) lines in both rotational progressions is indicative of a  $K = 0 \leftarrow 0$  band of a near-prolate symmetric top. Combination differences (rms deviation =  $0.00017 \text{ cm}^{-1}$ ) readily confirm that these transitions are due to  $(\text{HF})_2$  and allow an unambiguous  $J$  labeling and  $K''=0$  rotational assignment for both VRT bands. Furthermore, due to slight differences in the rotational constants for the two tunneling levels in the ground vibrational state, combination differences can also be used to assign the ground state vibration-tunneling symmetries ( $\Gamma_{\text{vib-tun}}$ ) for both bands.



J

Figure 5.2 A section of the spectrum of the  $K = 0 \leftarrow 0$  subband of the  $\nu_1 + \nu_4$  combination band ( $T_{\text{rot}} = 10 \pm 2$  K) of  $(\text{HF})_2$ . The  $A^+$  and  $B^+$  symmetry labels refer to  $\Gamma_{\text{vib-tun}}$ , the vibration-tunneling symmetry. Note the 10:6 spin statistical alternation in both bands and the narrow rovibrational linewidths ( $\Delta\nu \approx 30$  MHz). Additional small peaks are due to the multiquantum  $(11^11) \leftarrow (00^00)$  transitions of monomeric  $\text{N}_2\text{O}$  and a combination band of  $(\nu_1 + \nu_4)$  of the mixed dimer HFDF.

Table 5.1 The observed and fitted transition frequencies for  $\nu_4$  "van der Waals stretch" combination bands. The numbers in parentheses represent the deviations (obs – calc) from the least-squares fit of each VRT band in units of the last reported digit.

	$\nu_1 + \nu_4 K=0 \leftarrow 0$		$\nu_1 + \nu_4 K=1 \leftarrow 0$	$\nu_2 + \nu_4 K=0 \leftarrow 0$
	$B^+ \leftarrow A^+$	$A^+ \leftarrow B^+$	$B^+ \leftarrow A^+$	$A^+ \leftarrow B^+$
R(10)	4062.84645(4)			
R(9)	4062.48179(-7)			
R(8)	4062.11006(-10)			
R(7)	4061.73159(3)	4062.68837(11)	4103.6770(0)	
R(6)	4061.34634(8)	4062.31330(-3)	4103.2913(-7)	4002.9272(23)
R(5)	4060.95454(9)	4061.93054(-19)	4102.9010(4)	4002.5290(-4)
R(4)	4060.55639(8)	4061.54023(-37)	4102.5043(13)	4002.1265(-11)
R(3)	4060.15210(10)	4061.14321(15)	4102.0989(-3)	4001.7212(12)
R(2)	4059.74168(1)	4060.73840(18)	4101.6895(1)	4001.3059(-9)
R(1)	4059.32540(-2)	4060.32622(3)	4101.2728(-9)	4000.8880(-4)
R(0)	4058.90339(2)	4059.90692(-13)	4100.8528(9)	A
P(1)	4058.04217(-1)	4059.04771(-3)		3999.6040(5)
P(2)	4057.60321(5)	4058.60764(-3)	4099.5526(9)	3999.1643(-13)
P(3)	4057.15850(-8)	4058.16072(0)	b	3998.7230(1)
P(4)	4056.70835(-8)	4057.70696(5)	4098.6553(-9)	3998.2763(8)
P(5)	4056.25271(-2)	4057.24633(9)	b	3997.8246(14)
P(6)	4055.79136(-7)	4056.77876(3)	b	3997.3680(22)
P(7)	4055.32445(-7)	4056.30442(8)	b	3996.9004(-24)
P(8)	4054.85193(1)	4055.82328(21)		3996.4323(-23)
P(9)	4054.37358(2)	4055.33471(15)		
P(10)	4053.88924(-11)			
P(11)	4053.39929(11)			
Q(1)			c	
Q(2)			4100.4167(-8)	
Q(3)			4100.4111(3)	
Q(4)			4100.4016(-2)	
Q(5)			4100.3898(-7)	
Q(6)			4100.3775(6)	

a. too weak to observe

b. overlapped with a  $\nu_1 + \nu_5$  transition

c. unresolved

TABLE 5.2 Molecular constants ( $\text{cm}^{-1}$ ) determined from fits of the transition frequencies to Eq. (2) for combination bands assigned to the "van der Waals stretch" ( $\nu_4$ ) and "geared bend" ( $\nu_5$ ) intermolecular modes. All origins are with respect to the  $\Gamma_{\text{vib-tun}} = A^+$  tunneling level of the  $K = 0$  ground vibrational state of  $(\text{HF})_2$ . The uncertainties in parentheses represent  $2\sigma$  in the units of the last reported digit.

	$\nu_2 + \nu_4 \quad K = 0$	$\nu_1 + \nu_4 \quad K = 0$	$\nu_1 + \nu_4 \quad K = 1$	$\nu_2 + \nu_5 \quad K = 0$	$\nu_2 + \nu_5 \quad K = 1$	$\nu_1 + \nu_5 \quad K = 0$
$\Gamma_{\text{vib-tun}} =$	$A^+$	$B^+$	$B^+$	$A^+$	$A^+$	$B^+$
$\nu_0$	4000.6953(19)	4058.47560(6)	4100.4243(10)	4046.7466(4)	4088.6941(6)	4097.42616(8)
$\bar{B}$	0.21419(16)	0.213890(3)	0.21470(8)	0.21603(2)	0.21959(4)	0.214236(3)
$D/10^{-6}$	4.37(28)	2.821(22)	2.4(12)	1.97(22)	1.62(54)	1.75(2)
$b_K/10^{-3}$	----	----	3.57(8)	----	5.35(4)	----
$\sigma_{\text{rms}}$	0.00193	0.00007	0.0008	0.00047	0.00072	0.00011
$\Gamma_{\text{vib-tun}} =$	$B^+$	$A^+$	$A^+$	$B^+$	$B^+$	$A^+$
$\nu_0$	---- <sup>a</sup>	4060.13957(15)	---- <sup>a</sup>	4050.3335(8)	4095.2097(12)	4100.16527(8)
$\bar{B}$		0.213091(12)		0.21552(3)	0.21817(8)	0.213897(3)
$D/10^{-6}$		2.58(16)		2.06(28)	2.5(12)	2.09(2)
$b_K/10^{-3}$		----		----	4.93(6)	----
$\sigma_{\text{rms}}$		0.00016		0.00090	0.00090	0.00010

a. not observed

This spectroscopic assignment of  $\Gamma_{\text{vib-tun}}$  is quite clearly confirmed by the expected intensity alternation in  $J''$ . Specifically, the lines originating from the  $\Gamma_{\text{vib-tun}} = A^+ (B^+)$  level exhibit an approximately 10:6 (6:10) intensity alternation for even:odd  $J$  (for the  $K=0$  ground state). This is consistent with the known nuclear spin weights<sup>46</sup> for exchange of two pairs of equivalent spin 1/2 particles (i.e., H and F). Thus, the vib-tun symmetry assignments ( $\Gamma_{\text{vib-tun}} = \Gamma_{\text{vib}} \otimes \Gamma_{\text{tun}}$ ) are unambiguously corroborated both by the combination differences and nuclear spin statistics. All transitions from R(7) to P(9), inclusive, are observed for each of the two tunneling components and are listed in Table 5.1; the molecular constants obtained from a least squares fit to Eq. (5.2) are presented in Table 5.2. The standard deviations of the fits are  $\approx 0.0001 \text{ cm}^{-1}$ , which are comparable to the instrumental precision and indicate that no significant perturbations in the rovibrational transitions are present. Comparison of spectroscopic origins from the work of Bohac and Miller<sup>21</sup> yields fair agreement (within  $0.02 \text{ cm}^{-1}$ ) for both tunneling components, though this earlier study was limited by S/N and lower jet temperatures to only  $J < 4$  transitions. It is also worth noting that the primary emphasis of previous work was toward photofragment distributions rather than spectroscopic study of the intermolecular degrees of freedom.

Assignment of the intramolecular component of this combination band is based on a combination of linewidth and approximate tunneling symmetry arguments. As discussed previously, the energy ordering of a pair of tunneling levels provides information on the intramolecular vibrational symmetry of those two states. In essence, the energies of the two vibration-tunneling levels are

determined from the origins of the two VRT bands, the rigorous dipole selection rule for in-plane transitions ( $A^+ \leftrightarrow B^+$ ), and the known ground state tunneling splitting.<sup>8</sup> For the present band,  $\nu_K(\Gamma_{\text{vib-tun}} = A^+) > \nu_K(\Gamma_{\text{vib-tun}} = B^+)$  and thus, only a  $\nu_1$  intramolecular ( $\Gamma_{\text{intra}} = B^+$ ) assignment is consistent with an increase in total energy for an additional node in the tunneling wavefunction. Stated alternatively, the  $\nu_1$  assignment is consistent with a positive tunneling splitting.

Corroboration of this  $\nu_1$  intramolecular assignment can be obtained from a high resolution lineshape analysis (to be discussed in greater detail in section 5.4.4) of the individual rovibrational transitions. The transitions for each VRT band exhibit narrow contributions from predissociation broadening ( $\Delta\nu_{\text{pd}} = 25(5)$  MHz and  $40(8)$  MHz for  $\Gamma_{\text{vib-tun}} = A^+$  and  $B^+$ , respectively). This is qualitatively similar to the predissociation linewidths<sup>15</sup> observed in  $\nu_1$  ( $\Delta\nu_{\text{pd}} = 6.4(5)$  MHz and  $9.5(5)$  MHz for  $\Gamma_{\text{vib-tun}} = A^+$  and  $B^+$ , respectively) and considerably smaller than observed in  $\nu_2$  ( $330(30)$  MHz for both  $\Gamma_{\text{vib-tun}} = A^+$  and  $B^+$ ). Thus, the lineshapes also indicate a combination band built on the  $\nu_1$  intramolecular stretch. Indeed, in all 14 VRT bands observed in HF dimer to date, we find no exception to this pattern, i.e., there is a consistent correlation between linewidths in combination bands built on  $\nu_1$  or  $\nu_2$ , and the corresponding  $\nu_1/\nu_2$  fundamental excitations.

The intermolecular energy is determined by subtracting the origin of the parent HF fundamental from the combination band origin. In order to facilitate a more straightforward comparison with theoretical predictions, this is done consistently for the lower energy tunneling level ( $\Gamma_{\text{tun}} = A^+$ ) for both the fundamental and combination band state. The intermolecular vibrational energy

for this combination band is obtained by subtracting the  $\nu_1$  fundamental<sup>17</sup> ( $3930.9030(2) \text{ cm}^{-1}$ ) from the VRT band origin ( $4058.47560(6) \text{ cm}^{-1}$ ), yielding an intermolecular energy of  $127.5726(2) \text{ cm}^{-1}$ . As mentioned above, the two lowest intermolecular modes, i.e.,  $\nu_4$  and  $\nu_5$  have been historically assigned from theory as the "van der Waals stretch" and "geared bend", respectively, based on 2D cuts through the multidimensional eigenfunctions in order to locate nodes along the various degrees of freedom.<sup>28,54,55</sup> Comparison with *theoretical* predictions<sup>28</sup> on the intermolecular energy of the "van der Waals stretch" ( $126.37 \text{ cm}^{-1}$ ) provide strong circumstantial support for the  $\nu_4$  assignment.

However, a more experimentally based evaluation of these descriptive labels suggests otherwise. For  $\nu_1+\nu_4$  excitation ( $\Gamma_{\text{vib}} = \text{B}^+$ ), the spacing between the two VRT origins reflect the difference in upper and lower state tunneling splittings. Based on the known<sup>8,14,52</sup> ground state tunneling splitting of  $0.6586901(7) \text{ cm}^{-1}$ , the tunneling frequency in the upper state is  $1.6640(2) \text{ cm}^{-1}$ , a factor of  $\sim 7.7$  larger than the tunneling splitting in  $\nu_1$  ( $K = 0$ ) state. Such an increase in the tunneling frequency with  $\nu_4$  excitation is significantly larger than the factor of 2.2 predicted by full 6D QM theory,<sup>28</sup> and would be particularly surprising if this mode corresponds predominately to "van der Waals stretch" excitation. Conversely, since the "geared bend" motion correlates directly with motion along the tunneling coordinate, a dramatic enhancement of tunneling splitting with "geared bend" excitation is physically more reasonable and indeed predicted by full 6D QM calculations. Though we defer a more detailed discussion to Section 5, this is the first of several spectroscopic observations that reveal a significant degree of

"geared bend" character in the  $\nu_4$  state. As will be shown later, this interpretation is corroborated by a similar enhancement in the tunneling splitting observed in the corresponding  $\nu_5$  state.

### 5.3.2b ( $\nu_1 + \nu_4$ ) $K = 1 \leftarrow 0$

Based on the hybrid nature of the  $\nu_1$  excitation, one also anticipates an associated  $K = 1 \leftarrow 0$  perpendicular band for  $\nu_1 + \nu_4$ , spaced roughly one  $A_{eff}$  rotational constant ( $\sim 32 \text{ cm}^{-1}$ ) to the blue of the  $K = 0 \leftarrow 0$  parallel band origin at  $4058.5 \text{ cm}^{-1}$ . For the purposes of this discussion,  $A_{eff}$  is defined as the energy difference between the lower asymmetry split  $J = 1, K = 1$  and  $J = 0, K = 0$  states of a given vibrational level. Indeed, there is a weak (i.e., 0.5% of the integrated intensity of the  $K = 1 \leftarrow 0$   $\nu_1$  fundamental), red shaded Q-branch feature at  $\sim 4100 \text{ cm}^{-1}$  (see Figure 5.3), in the same region as the  $K = 0 \leftarrow 0$  parallel  $\nu_1 + \nu_5$  combination band. While the majority of the P-branch transitions overlap with the much stronger  $\nu_1 + \nu_5$  combination band (to be discussed in the next section), a moderately uncongested R-branch progression from R(0) to R(7) is observed. P/R branch combination differences ( $\sigma \leq 0.0005 \text{ cm}^{-1}$ ) calculated using two unobscured P-branch lines firmly establish an unambiguous  $J$  labeling of the transitions. In conjunction with an observed Q-branch and R(0), the spectrum is identified as a  $K = 1 \leftarrow 0$  perpendicular band. The combination differences, intensity alternation in the spectrum, and  $\nu_1$  intramolecular assignment are all consistent with a  $\Gamma_{\text{vib-tun}} = B^+ \leftarrow A^+$  VRT band. Similarly, the measured VRT transitions to the asymmetry

split  $K = 1$  upper state are consistent with an even parity vibration, or in the more common asymmetric top notation, a B-type band. The transition frequencies presented in Table 5.1 are fit to Eq. (5.2) using the  $A^+$  ground state constants; the molecular constants determined from this fit are in Table 5.2.

Observation of the other tunneling component for this weak combination band would further aid in the intramolecular assignment and also provide the tunneling splitting in the upper state. However, continuous scans 5-10  $\text{cm}^{-1}$  to either side of the lone VRT band origin ( $4100.4 \text{ cm}^{-1}$ ) do not reveal the other tunneling component. Based on the S/N for the observed VRT band this implies at least a 5-fold decrease in the peak transition strength for the  $\Gamma_{\text{vib-tun}} = A^+ \leftarrow B^+$  tunneling component. This difference is considerably larger than predicted by the relative Boltzmann populations of the lower tunneling levels at 10 K, and therefore either reflects a decrease in the transition strength and/or selective predissociation broadening for the  $A^+$  tunneling component of the  $\nu_1 + \nu_4$   $K = 1$  upper state.

Accurate measurements of the predissociation broadening for the observed transitions are difficult due to low S/N, yet estimates based on modeling the Q-branch structure indicate  $\Delta\nu_{\text{pd}}$  is approximately 75(50) MHz, i.e., more consistent with a  $\nu_1$  rather than  $\nu_2$  intramolecular assignment. Subtraction of the  $K = 0 \leftarrow 0$   $\nu_1$  origin gives an intermolecular energy of  $169.5213(10) \text{ cm}^{-1}$ . Given this  $K = 1$  state is approximately one  $A_{\text{eff}}$  ( $41.9487(10) \text{ cm}^{-1}$ ) to the blue of the  $\nu_1 + \nu_4$   $K = 0$  level, this band is tentatively assigned to the  $K=1 \leftarrow 0$  perpendicular band of  $\nu_1 + \nu_4$ . The substantial increase in  $A_{\text{eff}}$  compared to the  $\nu_1$  vibrational state ( $31.9630(2) \text{ cm}^{-1}$ ), would be surprising for a pure "van der Waals stretch," since this mode is not

predicted to have a large effect on the  $A$  axis moment of inertia. Conversely, a pure "geared bend" excitation involves large amplitude motion of the H atoms and thus is anticipated to have a pronounced effect on  $A_{eff}$ . We note for later discussion that the increases in  $A_{eff}$  observed for both  $\nu_4$  and  $\nu_5$  excitation are remarkably similar (41.9487 vs. 41.9475  $\text{cm}^{-1}$ ), suggesting again a strong mixing of van der Waals stretch/geared bend character in the two vibrational states.

### 5.3.2c ( $\nu_2 + \nu_4$ ) $K = 0 \leftarrow 0$

The assignment of the above series of combination bands to  $\nu_1 + \nu_4$  can be further corroborated by a search for the corresponding bands built on the  $\nu_2$  donor HF stretch. Indeed, another series of transitions (approximately 0.6% the transition strength of the  $\nu_2$   $K = 0 \leftarrow 0$  parallel band) are found near 4000  $\text{cm}^{-1}$ , approximately 60  $\text{cm}^{-1}$  to the red of the combination band assigned to  $\nu_1 + \nu_4$ ,  $K = 0 \leftarrow 0$ . This redshift is very close to the 62  $\text{cm}^{-1}$  frequency difference between the  $\nu_1$  and  $\nu_2$  fundamentals, thus strongly supporting a  $K = 0 \leftarrow 0$   $\nu_2 + \nu_4$  combination band assignment. Consistent with a  $\nu_2$  intramolecular assignment, the predissociation linewidths of these transitions are approximately 10-fold broader than the corresponding transitions for the  $\nu_1 + \nu_4$  combination band. The observed transitions presented in Table 5.1 are assigned unambiguously to originate from the upper ( $B^+$ ) tunneling level of the  $K = 0$  ground vibrational state, based on combination differences, which are confirmed by nuclear spin statistics. Results of the fit to these transition frequencies are presented in Table 5.2. Transitions from the other

tunneling component ( $A^+$ ) are not observed. This tunneling component must be down by at least a factor of 3 in peak transition strength, again presumably due to weaker transition strength and/or greater predissociation broadening.

Observation of both  $\nu_1+\nu_4$  and  $\nu_2+\nu_4$   $K = 0 \leftarrow 0$  parallel bands allows the intermolecular energies for the two excited intramolecular states to be compared directly. The intermolecular energy can be determined from the observed  $\nu_2+\nu_4$  tunneling component because it accesses the lower ( $\Gamma_{\text{tun}} = A^+$ ) tunneling level in the excited vibrational state. Subtraction of the  $\nu_2$  fundamental ( $3868.0793(2) \text{ cm}^{-1}$ ) yields an intermolecular frequency of  $132.6160(19) \text{ cm}^{-1}$ , which is close (within 4%) but noticeably higher than the  $127.57 \text{ cm}^{-1}$  frequency determined from the  $\nu_1+\nu_4$  combination band. This increase in intermolecular frequency is consistent with a greater "stiffening" of the intermolecular potential upon  $\nu_2$  versus  $\nu_1$  vibrational excitation, as will be discussed in greater detail in section 5.

### 5.3.3 $\nu_5$ ("Geared bend")

#### 5.3.3a $(\nu_1 + \nu_5) K = 0 \leftarrow 0$

The next higher intermolecular mode ( $\nu_5$ ) is predicted by 6D QM calculations<sup>28</sup> to be the "geared bend" around  $160.58 \text{ cm}^{-1}$ . Combination bands

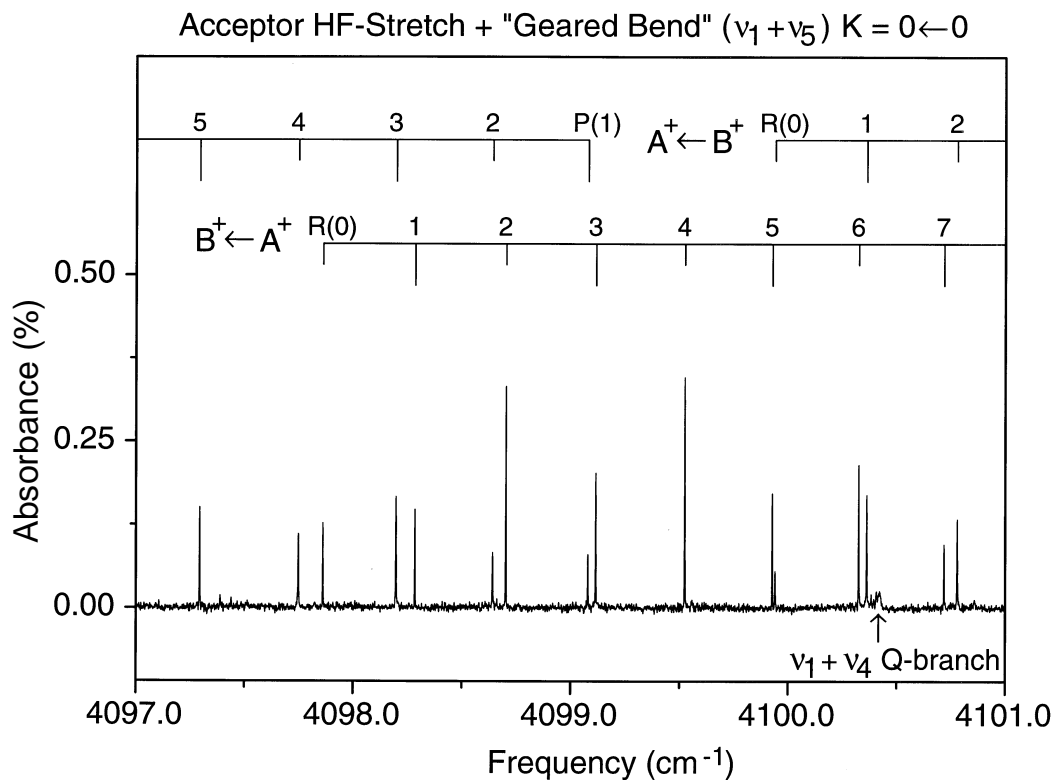


Figure 5.3 Spectral region near the origins of the two  $K=0 \leftarrow 0$  VRT bands of the  $\nu_1 + \nu_5$  combination band of  $(\text{HF})_2$ . The frequency differences between the two origins reflects the *difference* between the upper vibrational state and ground vibrational state tunneling splittings. The weaker feature at  $4100.4 \text{ cm}^{-1}$  is the Q-branch of the  $B^+ \leftarrow A^+$ ,  $K=1 \leftarrow 0$ ,  $\nu_1 + \nu_4$  combination band of  $(\text{HF})_2$ .

built on  $\nu_1$ , therefore, are expected in the vicinity of  $3931 + 161 = 4092 \text{ cm}^{-1}$ . Figure 5.3 shows a small section of a pair of overlapping bands (approximately 2% of the transition strength of the  $K = 1 \leftarrow 0 \nu_1$  fundamental) near  $4099 \text{ cm}^{-1}$ . The rovibrational transitions are readily assigned to the two tunneling components of the  $K'' = 0$  rotational state of HF dimer based upon ground state combination differences and nuclear spin statistics. All transitions from R(11) to P(12), inclusive, are observed for each VRT band and are listed in Table 5.3. The molecular constants obtained by fitting these transitions to Eq. (5.2) are listed in Table 5.2. In the upper vibrational state the energy of the  $\Gamma_{\text{vib-tun}} = A^+$  state is higher in energy than the  $B^+$  state, consistent with a  $B^+$  vibrational symmetry and thus, a combination band built on  $\nu_1$ . Furthermore, the  $\nu_1$  intramolecular nature of this combination state is confirmed by the narrow predissociation linewidths (20(5) MHz and 45(8) MHz for the  $\Gamma_{\text{vib-tun}} = A^+$  and  $B^+$  upper states, respectively) observed for both bands. By virtue of the parallel band structure and the spectroscopic data presented above, these two VRT bands are assigned to the two tunneling components of the  $K = 0 \leftarrow 0 \nu_1 + \nu_5$  combination band. Low  $J$  lines ( $J < 3$ ) out of the lower tunneling component were previously reported by Bohac and Miller,<sup>21</sup> though the slightly weaker (75%)  $A^+ \leftarrow B^+$  VRT band was not observed due to S/N limitations. Agreement with the previously reported  $B^+ \leftarrow A^+$  VRT band origin is good and within the limits of their reported uncertainties.

Given the  $\nu_1$  intramolecular assignment determined above, the intermolecular frequency is  $166.5232(2) \text{ cm}^{-1}$ . The tunneling frequency in the upper state,  $2.7391(11) \text{ cm}^{-1}$ , reflects a 13-fold increase in the tunneling splitting

Table 5.3 The observed and fitted transition frequencies for  $\nu_5$  "geared bend" combination bands. The numbers in parentheses represent the deviations (obs – calc) from the least-squares fit of each VRT band in units of the last reported digit.

	$\nu_1 + \nu_5 K=0 \leftarrow 0$		$\nu_2 + \nu_5 K=0 \leftarrow 0$		$\nu_2 + \nu_5 K=1 \leftarrow 0$	
	$B^+ \leftarrow A^+$	$A^+ \leftarrow B^+$	$B^+ \leftarrow A^+$	$A^+ \leftarrow B^+$	$B^+ \leftarrow A^+$	$A^+ \leftarrow B^+$
R(13)						
R(12)	4102.60216(-21)					
R(11)	4102.23466(27)	4104.27124(-12)				
R(10)	4101.86139(-8)	4103.90618(15)	4054.9330(-4)			
R(9)	4101.48364(8)	4103.53469(18)	4054.5297(8)	4050.3533(5)		
R(8)	4101.10055(-9)	4103.15766(8)	4054.1214(0)	4049.9317(-6)		
R(7)	4100.71262(-4)	4102.77467(10)	4053.7103(-9)	4049.5105(1)		4091.6206(4)
R(6)	4100.31960(-1)	4102.38570(-4)	4053.2974(-7)	4049.0870(-1)	4098.2508(-9)	4091.1607(-3)
R(5)	4099.92144(-3)	4101.99106(-3)	4052.8826(2)	4048.6625(0)	4097.8172(3)	4090.7038(-15)
R(4)	4099.51836(12)	4101.59079(3)	4052.4636(-4)	4048.2369(3)	4097.3825(5)	4090.2495(-11)
R(3)	4099.10993(0)	4101.18507(-3)	4052.0415(-14)	4047.8095(2)	a	4089.8003(-2)
R(2)	4098.69653(-1)	4100.77368(-5)	4051.6195(2)	4047.3807(0)	4096.5143(19)	4089.3547(-8)
R(1)	4098.27808(-2)	4100.35673(-1)	4051.1923(-9)	4046.9511(2)	4096.0780(3)	4088.9110(-3)
R(0)	4097.85462(-1)	4099.93436(-9)	4050.7662(16)	4046.5199(-1)	4095.6430(-5)	4088.4716(7)
P(1)	4096.99276(2)	4099.07358(16)	4049.8992(-9)	4045.6542(-6)		4087.1732(11)
P(2)	4096.55446(4)	4098.63505(14)	4049.4646(3)	4045.2200(-7)		a
P(3)	4096.11127(2)	4098.19135(1)	4049.0260(-3)	4044.7856(2)		a
P(4)	4095.66331(0)	4097.74223(-18)	4048.5867(6)	4044.3499(5)		4085.9045(0)
P(5)	4095.21072(7)	4097.28831(15)	4048.1440(3)	4043.9128(4)		a
P(6)	4094.75339(2)	4096.82894(-3)	4047.7002(11)	4043.4754(7)		4085.0781(4)
P(7)	4094.29145(-9)	4096.36474(-13)	4047.2517(-7)	4043.0362(0)		
P(8)	4093.82513(-14)	4095.89503(-6)	4046.8052(14)	4042.5960(-9)		
P(9)	4093.35446(-20)	4095.42096(-22)		4042.1570(0)		
P(10)	4092.87990(7)	4094.94198(12)				
P(11)	4092.40109(20)	4094.45766(-2)				
P(12)	4091.91803(5)	4093.96854(-12)				
P(13)	4091.43122(-2)					
Q(1)					b	4088.0450(9)
Q(2)					4095.2247(-11)	4088.0617(1)
Q(3)					4095.2417(-1)	4088.0881(3)
Q(4)					4095.2631(-2)	4088.1227(-1)
Q(5)					4095.2898(-1)	4088.1677(10)
Q(6)					4095.3211(-7)	4088.2200(7)
Q(7)					4095.3588(1)	4088.2806(-3)
Q(8)					4095.4013(5)	4088.3515(-1)
Q(9)						4088.4309(-4)

a. too weak to observe

b overlapped with P(5) of  $\nu_1 + \nu_5 B^+ \leftarrow A^+$

from  $\nu_1 (K=0)$  state. Such a large increase in the tunneling frequency is consistent

with considerable "geared bend" nature in the  $\nu_5$  excitation, since this motion

correlates strongly with the tunneling coordinate. However, as noted above, a comparably large increase in tunneling splitting (8-fold) is also observed between  $\nu_1+\nu_4$  and  $\nu_1$  excitation, which again suggests strongly mixed "van der Waals stretch" and "geared bend" character in each of  $\nu_4$  and  $\nu_5$  intermolecular modes.

### 5.3.3b ( $\nu_2 + \nu_5$ ) $K = 0 \leftarrow 0$

Based on a  $\nu_1+\nu_5$  intramolecular assignment for the combination band above, then the  $\nu_5$  intermolecular mode should also be observable built on  $\nu_2$ . Figure 5.4 shows a section of a parallel band (~2% of the transition strength of the  $\nu_2$   $K = 0 \leftarrow 0$  fundamental) near  $4046 \text{ cm}^{-1}$ , i.e., approximately  $47 \text{ cm}^{-1}$  to the red of the  $\nu_1+\nu_5$  combination band. This shift is close to (but, as in the previous comparison between  $\nu_1+\nu_4$  and  $\nu_2+\nu_4$ , slightly lower than) the  $62 \text{ cm}^{-1}$  difference between the  $\nu_1$  and  $\nu_2$  fundamentals, and thus offers strong confirmation that this is the  $K = 0 \leftarrow 0$  parallel combination band of the  $\nu_5$  intermolecular mode built on  $\nu_2$ . As evident from inspection of Figure 5.4, the predissociation linewidths for these transitions are approximately 10-fold broader (270(20) MHz) than the corresponding  $\nu_1+\nu_5$  transitions, in further support of the  $\nu_2+\nu_5$  mode assignment. All the observed transition frequencies for both tunneling states are listed in Table 5.3.

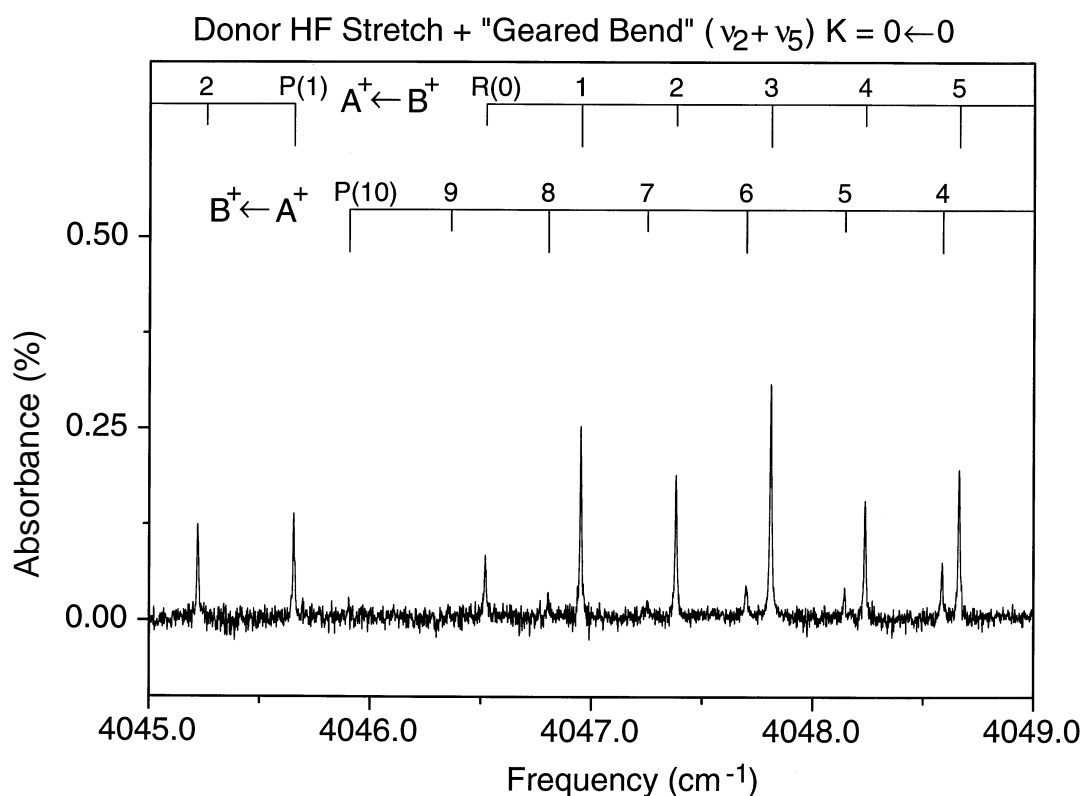


Figure 5.4 A section of the infrared absorption spectrum of  $(\text{HF})_2$  displaying the  $K = 0 \leftarrow 0$   $\nu_2 + \nu_5$  combination band. The origins for these two VRT bands are widely spaced because they correspond to the *sum* of tunneling splittings in lower and upper vibrational states. The broad rovibrational lineshapes ( $\Delta\nu_{\text{pd}} \approx 300$  MHz) are very different from the transitions shown in figures 2 or 3; this is consistent with this band being built on  $\nu_2$  instead of  $\nu_1$ .

Combination differences with the  $K = 0$  ground state verify the  $J$  labeling and tunneling assignment for each VRT band, which again are confirmed by the nuclear spin statistics. The molecular constants determined from fits of the transition frequencies to Eq. (5.2) are presented in Table 5.2. The energy ordering of the tunneling levels indicates a  $\Gamma_{\text{vib}} = A^+$  vibrational symmetry, which is consistent with the  $\nu_2$  intramolecular assignment first deduced from the predissociation linewidths. Low  $J$  transitions in both tunneling components of this band were previously reported by Bohac and Miller,<sup>21</sup> with approximate origins and an upper state tunneling splitting inferred. However, agreement with the previously reported values is not good: though the  $B^+ \leftarrow A^+$  band originating from the *lower* tunneling level is in fair agreement ( $0.02 \text{ cm}^{-1}$ ) with the present value, neither the origin nor the reported transition frequencies of the  $A^+ \leftarrow B^+$  band are within  $2 \text{ cm}^{-1}$  of the current measurements. The rotational spacings previously observed by Bohac and Miller in this second band clearly identify HF dimer as the carrier. However, we observe no transitions under the slit jet expansion conditions that match the initially reported values, even though the S/N on the correct  $A^+ \leftarrow B^+$  band is easily 20:1 even near the origin (see Fig 5.4).

The  $\nu_5$  intermolecular frequency is determined to be  $178.6673(4) \text{ cm}^{-1}$  by subtracting the  $\nu_2$  fundamental frequency. This  $\nu_5$  intermolecular energy is close to but 7% greater than the value determined from the  $\nu_1 + \nu_5$  combination band ( $166.52 \text{ cm}^{-1}$ ), as anticipated from the  $\nu_1 + \nu_4$  and  $\nu_2 + \nu_4$  comparison presented earlier. For an upper vibrational state with  $\Gamma_{\text{vib}} = A^+$  symmetry, the *difference* in the origins of the two VRT bands corresponds to the *sum* of splittings in the lower and upper

vibrational states; the tunneling splitting in the  $\nu_2+\nu_5$   $K = 0$  excited state is therefore  $3.5868(9) \text{ cm}^{-1}$ . This represents a 17-fold increase from the  $\nu_2$  state, i.e., similar to the 13-fold increase observed between the  $\nu_1$  and  $\nu_1+\nu_5$  states. Indeed, this larger enhancement in the tunneling splitting for the higher energy  $\nu_5$  mode ( $179 \text{ cm}^{-1}$  vs.  $167 \text{ cm}^{-1}$ ) is expected, as will be discussed in section 5. Due to the present re-assignment of the  $A^+ \leftarrow B^+$  VRT band, the intermolecular frequency and tunneling splitting differ significantly from the values ( $\nu_5 = 180.16 \text{ cm}^{-1}$ ,  $\Delta\nu_{\text{tun}} = 1.2 \text{ cm}^{-1}$ ) estimated previously.<sup>21</sup>

### 5.3.3b ( $\nu_2 + \nu_5$ ) $K = 1 \leftarrow 0$

If there is any appreciable perpendicular character to the  $\nu_2+\nu_5$  transition, then by analogy to  $\nu_1+\nu_4$  there should be an additional pair of  $K = 1 \leftarrow 0$  tunneling bands shifted by approximately  $A_{\text{eff}}$  to the blue of the  $\nu_2+\nu_5$   $K = 0 \leftarrow 0$  origin, i.e., near  $4090 \text{ cm}^{-1}$ . Furthermore, due to the sensitivity of the tunneling splitting both to intermolecular energy and  $K$  excitation,<sup>12,15</sup> a  $K = 1$  "geared bend" intermolecular state near  $220 \text{ cm}^{-1}$  should exhibit a significantly enhanced tunneling splitting.

Consistent with these expectations, there are two widely separated Q-branch features (0.4% of the  $\nu_2$  fundamental transition strength) with blue shaded origins near  $4088$  and  $4095 \text{ cm}^{-1}$  (see Fig. 5). Closer inspection of the band at  $4088 \text{ cm}^{-1}$  reveals the corresponding R- and P-branch transitions which are listed in Table 5.3. From combination differences and  $J$ -dependent intensity

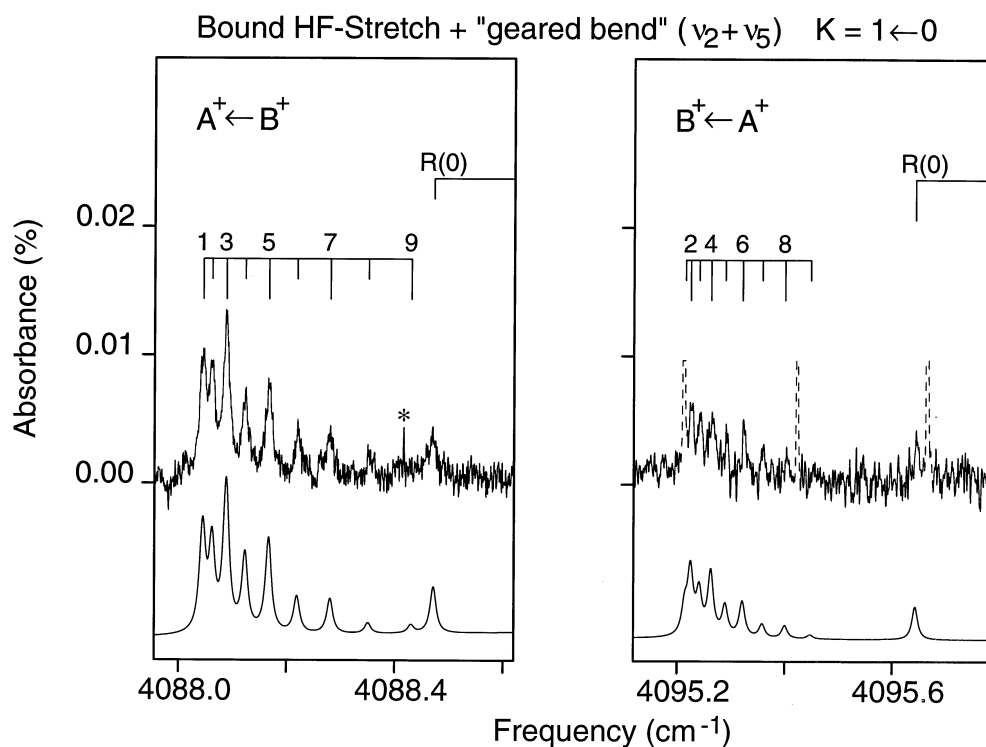


Figure 5.5 A portion of spectrum (upper trace) near the two Q-branches of the weak  $K=1 \leftarrow 0$   $\nu_2 + \nu_5$  combination band of  $(\text{HF})_2$ . To provide a clear view of the  $B^+ \leftarrow A^+$  VRT band, strong  $K=0 \leftarrow 0$   $\nu_1 + \nu_5$  transitions present in the spectrum are truncated and dashed. The lower trace is the simulated spectrum calculated by modeling the Q-branch structure with a sum of Voigt profiles (see text for details). The homogeneous (lifetime) broadening of the lineshapes for each VRT band are determined to be 390(50) and 290(75) MHz for the  $A^+$  and  $B^+$  upper states, respectively, consistent with the  $\nu_2$  intramolecular assignment. The sharp transition marked with an asterisk is due to a combination band of ArHF.

alternations, these transitions are determined to originate from the upper ( $B^+$ ) tunneling level of the ground vibrational state. The band at  $4095\text{ cm}^{-1}$  is slightly weaker and only the corresponding R-branch has been positively identified. However, the R and Q branch features (listed in Table 5.3), could be unambiguously assigned to the  $A^+$  lower tunneling state by inspection of the spin statistics. The  $J$  labeling for the R-branch of this VRT band is based on line spacing with respect to the central Q-branch, as confirmed by the rotational least squares fits. Thus, these two  $B^+ \leftarrow A^+$ ,  $A^+ \leftarrow B^+$  bands correspond to a tunneling pair of a combination band with an unusually large tunneling splitting. The results of fits to Eq. (5.2) for each VRT band are presented in Table 5.2.

The two VRT bands are assigned to the  $K = 1 \leftarrow 0$  perpendicular band of  $\nu_2 + \nu_5$  based on a variety of spectral evidence. First, the bands originate from the two tunneling levels of the  $K = 0$  ground vibrational state; the presence of Q-branches in both VRT bands therefore clearly establishes the  $K = 1 \leftarrow 0$  perpendicular band assignment. Secondly, the relative ordering of the two VRT band origins ( $\nu_K(B^+ \leftarrow A^+) > \nu_K(A^+ \leftarrow B^+)$ ) indicates  $\Gamma_{\text{vib}} = A^+$ , consistent with a  $\nu_2$  intramolecular vibration. This intramolecular assignment is confirmed by the noticeably broadened predissociation linewidths (approximately 300 MHz) in each band, characteristic of a combination band built on  $\nu_2$  versus  $\nu_1$  (see Figure 5.5.). The  $\nu_5$  "geared bend" intermolecular assignment is supported by the large tunneling splitting,  $6.5153(13)\text{ cm}^{-1}$ , determined for this state, since both "geared bend" and  $K$  excitation are known<sup>12,15,21</sup> to increase the tunneling splitting. Finally, subtraction of the  $\nu_2$  fundamental yields an intermolecular vibrational frequency of

220.6148(6)  $\text{cm}^{-1}$  for the  $K = 1$  state, which is 41.9475(7)  $\text{cm}^{-1}$  (i.e., essentially  $A_{eff}$ ) higher in intermolecular energy than the  $\nu_2+\nu_5$  ( $K=0\leftarrow 0$ ) band.

As mentioned earlier, the term values for excited  $K$  levels can be highly quantum state dependent due to large amplitude motion of the H atoms. In the  $\nu_2+\nu_5$  state, for example,  $A_{eff} = 41.95 \text{ cm}^{-1}$  is 30% larger than in the  $\nu_2$  ( $A_{eff} = 32.13 \text{ cm}^{-1}$ ) state. The increase in  $A_{eff}$  with "geared bend" excitation is expected from vibrational averaging arguments, and is indeed confirmed by QM calculations. The possible extremes range from  $A_{eff} = \text{infinity}$  for the perfectly linear complex, down to a minimum of only  $A_{eff} \approx 10 \text{ cm}^{-1}$  (i.e.,  $B_{HF}/2$ ) for a "rectangular" geometry. Physically, the effect of "geared bend" excitation on the  $A$  axis moment of inertia skews the average to *larger*  $A_{eff}$  values due to the predominance of contributions from configurations approaching a more linear structure. This is also supported from 4D QM calculations<sup>36</sup> for both  $K = 0$  and  $K = 1$  states, where "geared bend" excitation is found to increase the  $K = 1\leftarrow 0$  spacing by approximately 30%, in good agreement with experiment.

## 5.5 Discussion

### 5.5.1 Intramolecular vibrational dependence of the intermolecular frequencies

It has long been known from fundamental redshifts observed by Pine *et al.*<sup>17</sup> that  $(\text{HF})_2$  is more tightly bound in the  $\nu_1$  and  $\nu_2$  intramolecular *excited* states, and that this increase is greater for  $\nu_2$  versus  $\nu_1$  excitation. Indeed, the small shifts in

intermolecular frequencies between the  $\nu_1$  and  $\nu_2$  supported states provide an alternate measure of this differential "stiffening" of the hydrogen bond with intramolecular excitation. For example, in each of the two cases where an intermolecular mode is observed in combination with *both*  $\nu_1$  or  $\nu_2$ , the  $\nu_2$  supported intermolecular levels are systematically *higher* in energy than the corresponding  $\nu_1$  supported levels. This trend is consistent with the more strongly redshifted  $\nu_2$  donor (2.4%) relative to the  $\nu_1$  acceptor stretch (0.8%), and furthermore suggests there may be a useful correlation between *intramolecular redshifts* and *intermolecular frequencies*. Of particular interest, therefore, is whether the intermolecular energies determined from combination bands for the intramolecular excited states can be used to predict the analogous intermolecular states on the ground intramolecular surface.

As a test of this hypothesis, the measured values of  $\nu_4$  built on  $\nu_1$  (127.57  $\text{cm}^{-1}$ ) and  $\nu_2$  (132.62  $\text{cm}^{-1}$ ) are plotted as a function of intramolecular redshift in Figure 5.6. Also plotted at zero redshift is the  $\nu_4$  value (125(5)  $\text{cm}^{-1}$ ) inferred from far-IR data,<sup>24</sup> i.e., where only intramolecular zero point excitation is present. It is evident that the intermolecular frequencies upon intramolecular excitation are remarkably well correlated with the magnitude of the intramolecular redshift. Indeed, the 125.1(1)  $\text{cm}^{-1}$   $\nu_4$  intermolecular frequency predicted from a simple linear extrapolation of the  $\nu_1/\nu_2$  combination band data agrees to well within the 5  $\text{cm}^{-1}$  uncertainty of the experimentally determined far-IR value. This near linear dependence between intermolecular frequency and redshift bodes well for quantitative predictions of far-IR results from the present combination band data.

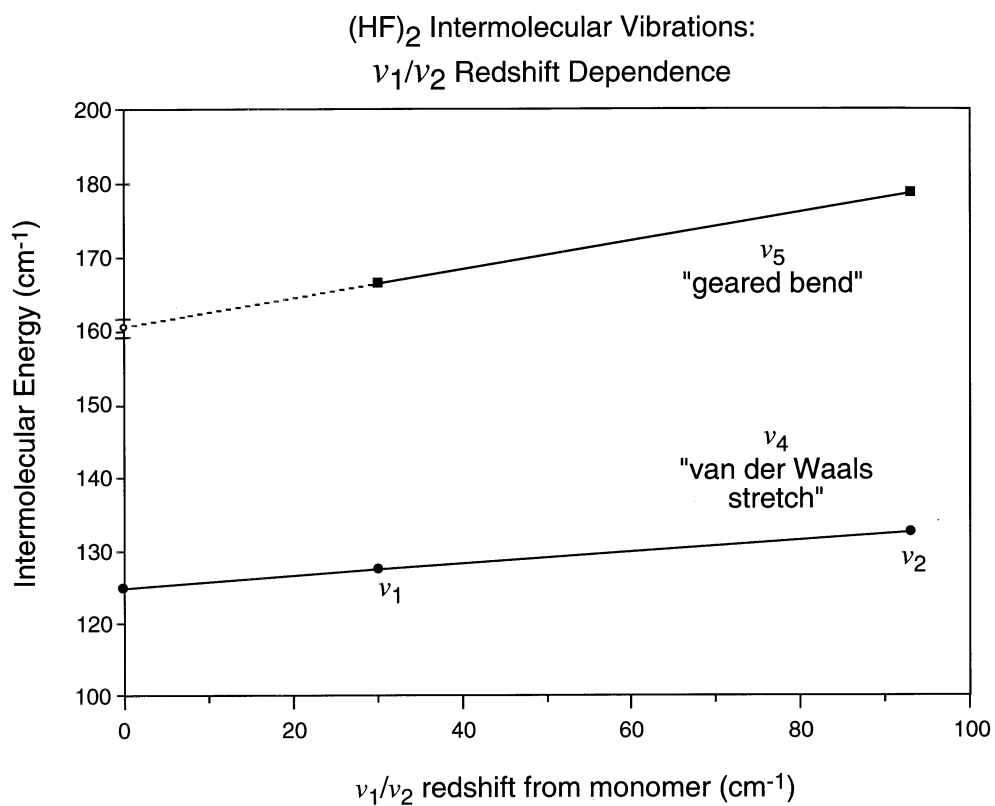


Figure 5.6 Plot of the  $\nu_4/\nu_5$  intermolecular energies as a function of intramolecular redshift. Extrapolation of the  $\nu_5$  data to zero redshift predicts a far-IR transition frequency at  $160.6(6) \text{ cm}^{-1}$  (error estimated from the uncertainties in the intermolecular energies).

Table 5.4 The  $\nu_4$  and  $\nu_5$  intermolecular energies ( $\text{cm}^{-1}$ ) determined from the  $\nu_1/\nu_2$  combination bands. Far-IR intermolecular fundamentals are included along with the extrapolated values from figure 6. The uncertainties in parentheses are in units of the last reported digit. Theoretical predictions (4D and 6D) for the far-IR frequencies are discussed in the text.

	$K$	Near-IR $\nu_2$	Near-IR $\nu_1$	Far-IR	Theory 4D <sup>a</sup>	Theory 6D <sup>b</sup>
redshift <sup>c</sup>		-93.3432	-30.5195	----		
$\nu_4$	0	132.6160(19)	127.5726(2) [127.549(1)] <sup>e</sup>	125.1(1) <sup>d</sup> [125(5)] <sup>f</sup>	125.38	126.37
	1	----	169.5213 (10)	----	167.91	----
$\nu_5$	0	178.6673(4) [180.16(1)] <sup>e</sup>	166.5232(2) [166.518(1)] <sup>e</sup>	160.6(6) <sup>d</sup>	160.16	160.58
	1	220.6148(6)	----	----	214.27	----

a. Reference 36

b. Reference 38

c. shift from the HF monomer origin at  $3961.422490 \text{ cm}^{-1}$ .

d. far-IR extrapolations from fig 6.

e. Reference 21

f. Reference 24

For example, the measured values for  $\nu_5$  built on  $\nu_1$  and  $\nu_2$  are also plotted in Figure 5.6; extrapolation to zero redshift predicts a far-IR value of  $160.6(6) \text{ cm}^{-1}$  for the corresponding  $\nu_5$  intermolecular fundamental. This mode has not yet been seen in the far-IR, though there has been a tentative assignment<sup>14</sup> of one tunneling component of the much higher frequency  $\nu_5$   $K = 3 \leftarrow 2$  band at  $394 \text{ cm}^{-1}$ .

Unfortunately,  $A$  axis rotation contributions to the intermolecular energies at these high  $K$  levels are significantly greater than the  $\nu_5$  energy itself, and thus

extrapolation from the far-IR data to the  $\nu_5 K = 0$  level is not quantitatively reliable. This prediction should therefore be useful in guiding far-IR spectral searches, and also to compare with QM calculations on trial potential energy surfaces, as described below.

The extrapolated values of  $\nu_4/\nu_5$  determined from Fig 5.6 are compared to two sets of calculations performed by Zhang *et al.*, based on the SQSBDE surface of Quack and Suhm.<sup>24</sup> In the first calculations<sup>36</sup> the HF intramolecular coordinates are held fixed at vibrationally averaged ground state values, and the resulting 4D intermolecular eigenstates are calculated using a body-fixed variational method. The only other dynamical approximation is to neglect Coriolis interactions (i.e., helicity decoupling), which is anticipated to be a good approximation in general for  $(\text{HF})_2$  and is rigorous for  $J = 0$  states. The second set reflect full 6D coupled calculations<sup>28</sup> for the ground intramolecular states and thus are "exact" for a given PES. Both sets of results are summarized in Table 5.4 and reveal quite reasonable agreement between the calculated and observed values for all  $\nu_4$  and  $\nu_5$  states observed. The excellent agreement (<1%) between the extrapolated values and the 6D QM calculations represents a significant success of the SQSBDE potential surface for describing the intermolecular dynamics in the ground HF-stretching states. The slight differences between the 4D and 6D calculations provide clear evidence that all  $3N-6$  degrees of freedom must be tackled for comparison at any spectroscopic level of precision, but the 4D calculations offer a useful first test of how accurately the intermolecular frequencies are reproduced. In order to probe the full dimensionality of the PES in more detail, especially given the new

combination band data for the  $\nu_4/\nu_5$  intermolecular frequencies in the  $\nu_1/\nu_2$  states, full 6D calculations of the intermolecular frequencies in *excited* HF-stretch states will clearly be necessary. Recent results along these lines will be discussed toward the end of this section.

#### 5.4.2 Effect of intermolecular excitation on rotational constants

The good agreement between theory and the extrapolated intermolecular frequencies provides strong support that the basic topology of the HF dimer PES is correct. If we pursue this comparison with quantities more sensitive to eigenfunctions than simply eigenvalues, however, discrepancies begin to be apparent. An appropriate place to start is with the  $\bar{B}$  and  $A_{eff}$  rotational constants measured for the different intermolecular states, since these quantities are preferentially sensitive to (i) average HF-HF center of mass separation and (ii) angular orientation of the H-atoms, respectively. We can focus on the effect of intermolecular excitation by investigating *ratios* of combination state  $\bar{B}$  and  $A_{eff}$  constants to the corresponding values for the  $\nu_1$  or  $\nu_2$  excited states. This also directly addresses the issue of mixing between the low frequency van der Waals stretch and geared bend degrees of freedom, which is indicated by much of the current spectroscopic data discussed below.

The change in the  $\bar{B}$  rotational constant with intermolecular excitation is dominated by the change in  $\langle 1/R^2 \rangle$ , where R is the center of mass separation between the two HF molecules. Though the expectation values of  $1/R^2$  are not

Table 5.5 The  $\bar{B}$  and  $A_{eff}$  rotational constants for  $\nu_1$  and  $\nu_2$  excited HF-stretching states of (HF)<sub>2</sub>, including states with  $\nu_4/\nu_5$  intermolecular excitation. The measured changes in rotational constants upon intermolecular excitation are compared to theoretical predictions.

$\Gamma_{\text{vib-tun}} =$	$\bar{B}$ (cm <sup>-1</sup> )				$\Delta\bar{B}$ (%)	
	$\nu_1 K = 0$		$\nu_2 K = 0$		Expt (Average)	Theory <sup>a</sup>
	B <sup>+</sup>	A <sup>+</sup>	A <sup>+</sup>	B <sup>+</sup>		
---- <sup>b</sup>	0.217923(1) <sup>c</sup>	0.217869(1) <sup>c</sup>	0.219019(1) <sup>d</sup>	0.218952(1) <sup>d</sup>	----	----
$\nu_4$	0.213890(3)	0.21309(1)	0.21419(16)	----	-2.3(1)	-4.2
$\nu_5$	0.214236(3)	0.213897(3)	0.21603(2)	0.21959(4)	-1.6(1)	-1.2

$\Gamma_{\text{vib-tun}} =$	$A_{eff}$ (cm <sup>-1</sup> )			$\Delta A_{eff}$ (%)	
	$\nu_1$	$\nu_2$	4D QM	Expt	Theory <sup>e</sup>
	B <sup>+</sup>	A <sup>+</sup>	A <sup>+</sup>		
---- <sup>b</sup>	31.9630(2) <sup>d</sup>	32.1315(8) <sup>d</sup>	39.93	----	----
$\nu_4$	41.9487(10)	----	42.63	32.24(1)	6.76
$\nu_5$	----	41.9475(7)	54.11	30.55(1)	35.5

- Reference 38
- intermolecular ground state
- Reference 12
- Reference 17
- Reference 36

available, Zhang *et al.*<sup>28</sup> do report  $\langle R \rangle$  values for each quantum state in the 6D QM calculations discussed above. The calculations predict a 2.1% increase in  $\langle R \rangle$  for  $\nu_4$  excitation while only a 0.6% increase for  $\nu_5$  excitation. The clear differences in  $\langle R \rangle$  with  $\nu_4$  vs.  $\nu_5$  ("van der Waals stretch" vs. "geared bend") excitation demonstrate that the PES treats these motions as largely decoupled, though the 0.6% increase in  $\langle R \rangle$  for  $\nu_5$  does already indicate some degree of stretch-bend mixing. Since these are small fractions of  $\langle R \rangle$ , the value of  $\bar{B}$  would be predicted

to decrease by approximately -4.2% in the  $\nu_4$  state and only -1.2% in the  $\nu_5$  excited state, i.e., a 3.5 fold difference. On the other hand, if both the  $\nu_4$  and  $\nu_5$  intermolecular modes are better described as a more equivalent admixture of van der Waals stretch and geared bend character, then the changes in  $\bar{B}$  should be roughly equivalent and halfway between these two extremes. As shown in the upper half of Table 5.5, the experimental decreases in  $\bar{B}$  are (i) quite similar for both intermolecular modes (-2.3% and -1.6%) and (ii) intermediate between the predicted values, i.e., more consistent with a model of strongly mixed van der Waals stretch and geared bend character in the  $\nu_4/\nu_5$  manifold.

The eigenvalues for the  $J = 1, K = 1$  and  $J = 0, K = 0$  states (see Table 5.4) allow  $A_{eff}$  to be calculated directly, which provides another eigenfunction sensitive probe of the angular vs. radial motion associated with a given intermolecular state. The experimentally determined values of  $A_{eff}$  along with the predictions based on the 4D QM calculations<sup>36</sup> are presented in the lower half of Table 5.5. Similar to the analysis of  $\Delta\bar{B}$ , the fractional changes in  $A_{eff}$  for the theoretically predicted intermolecular modes differ by 5.3-fold in magnitude, while experimentally the changes are found to be nearly equivalent (i.e., within 5%). Specifically, the QM calculations predict that excitation of  $\nu_4$  ("van der Waals stretch") has little effect on  $A_{eff}$ , while  $\nu_5$  ("geared bend"), which involves large amplitude angular motion of the two HF moieties, increases  $A_{eff}$  substantially. Physically, the large increases in  $A_{eff}$  found experimentally for *both* intermolecular modes again suggests considerable angular motion associated with *both*  $\nu_4$  and  $\nu_5$ .

### 5.4.3 Donor-acceptor interchange tunneling

Intermolecular excitation is predicted to increase the donor-acceptor tunneling rate in a strongly mode specific fashion. A large body of theoretical work<sup>17,24,28,31-33,36,50,52,54-58</sup> has been directed at describing the HF dimer energy level splittings and the 6D calculations presented above for the ground HF-stretch vibrational states predict that both the  $\nu_4$  "van der Waals stretch" and  $\nu_5$  "geared bend" should enhance the tunneling rate by factors of 2 and 17, respectively. The geared bend intermolecular mode is predicted to exhibit the larger effect since this mode correlates strongly with the tunneling coordinate over a  $C_{2h}$  transition state. Quantitative predictions for the tunneling splittings in states that include one quantum of intramolecular excitation (i.e., which are measured in the present combination band study) are not yet available. However, one would similarly anticipate a strong preferential enhancement of tunneling rates for eigenfunctions with significant components of geared bend versus van der Waals stretch motion.

For purposes of comparison, we can attempt to isolate this effect of intermolecular excitation on tunneling by examination of the ratio of the observed combination state splitting to the corresponding  $\nu_1$  or  $\nu_2$  excited state value for a given  $K$  level. The relevant tunneling splittings and ratios measured in this study for  $\nu_1$  and  $\nu_2$  excited states, along with the ratios predicted for ground intramolecular states, are presented in Table 5.6. Examination of the  $\nu_1$  data in Table 5.6 reveals that both intermolecular modes enhance the tunneling rate dramatically, leading to excited state splittings on the order of  $2 \text{ cm}^{-1}$ , i.e.,

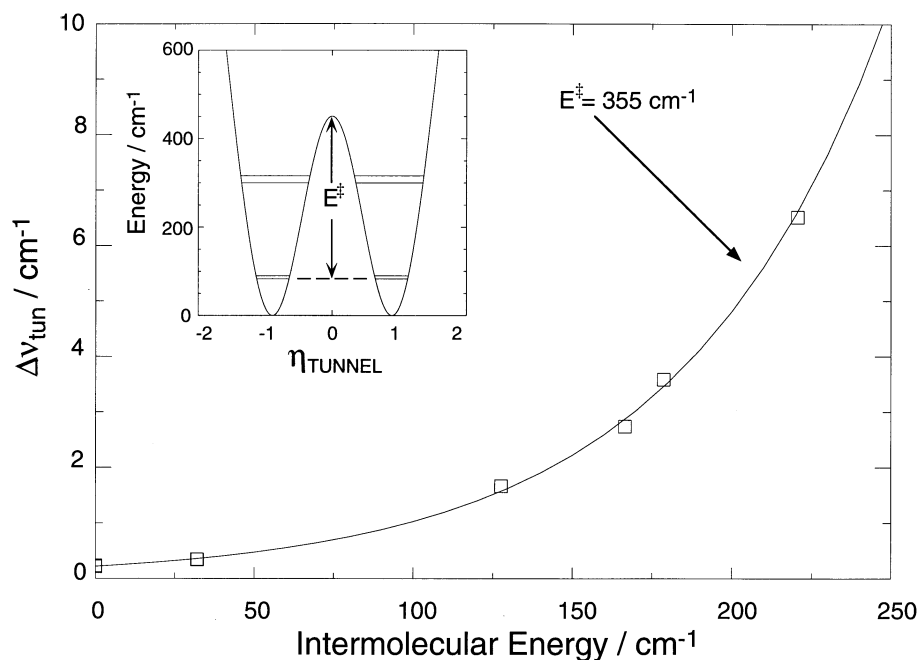
(HF)<sub>2</sub> Intermolecular Modes: 1D WKB Tunneling Analysis of  $\nu_4/\nu_5$ 

Figure 5.7 Plot of the observed tunneling splittings versus intermolecular energy along with a least squares fit to Eq. (3). The inset shows a cartoon of the effective 1D tunneling potential used in the WKB analysis along with a definition of the barrier height,  $E^\ddagger$ . The effective 1D barrier height ( $E^\ddagger$ ) is  $355(2) \text{ cm}^{-1}$  where the reported uncertainty reflects the fit, not the simplifying approximations of a 1D tunneling model.

Table 5.6 Tunneling splittings  $\Delta\nu_{\text{tun}}$  ( $\text{cm}^{-1}$ ) measured in HF-stretch excited states from the combination band data. The ratio of the observed combination state splittings with the corresponding  $\nu_1$  or  $\nu_2$  excited state values are in parentheses. Theoretical predictions for the effect of  $\nu_4/\nu_5$  intermolecular excitation are also included to allow comparison.

	$\nu_1$ acceptor-HF		$\nu_2$ donor-HF		Theory (4D) <sup>a</sup>	
	$K=0$	$K=1$	$K=0$	$K=1$	$K=0$	$K=1$
---- <sup>b</sup>	0.2155 <sup>c</sup>	0.3499 <sup>c</sup>	0.2334 <sup>c</sup>	0.3411 <sup>c</sup>	0.48	0.86
$V_4$	1.6640 (7.72)	----- <sup>d</sup>	----- <sup>d</sup>		1.11 (2.31)	1.45 (1.68)
$V_5$	2.7391 (12.7)		3.5868 (15.4)	6.5153 (19.1)	7.97 (16.6)	18.65 (21.7)

<sup>a</sup> Reference 37

<sup>b</sup> ground intermolecular state

<sup>c</sup> Reference 17

<sup>d</sup> Only one tunneling level observed.

between 8- to 13-fold larger than the corresponding  $0.2 \text{ cm}^{-1}$  tunneling splittings in  $\nu_1$  or  $\nu_2$ . However, although the sign and magnitude of these ratios are in good qualitative agreement with theoretical predictions, there is far less mode selectivity observed than anticipated. Specifically, the observed increase in the tunneling splitting for  $\nu_4$  is *greater* than predicted while the observed increase for  $\nu_5$  excitation is *less* than predicted. This is again consistent with the strong mixing of "van der Waals stretch" and "geared bend" modes predicted from the previous analysis of the rotational constants.

The degree of mode mixing in  $\nu_1+\nu_4$  and  $\nu_1+\nu_5$  can be quantified via the following simple two state analysis. From a two state perspective, we consider

tunneling in two zero order "van der Waals stretch" and "geared bend" states, with values  $\Delta v_{\text{tun}}^{\text{vdw}}$  and  $\Delta v_{\text{tun}}^{\text{geared}}$ , respectively. As a reasonable first estimate, these uncoupled, zero order states would be quite similar to those predicted from the 4D QM calculations,<sup>36</sup> which yield a mode specific enhancement ratio of  $\Delta v_{\text{tun}}^{\text{geared}} / \Delta v_{\text{tun}}^{\text{vdw}} = 7.2$ . In the presence of off diagonal coupling ( $\gamma$ ), the  $\nu_4$  and  $\nu_5$  tunneling splittings for the experimentally observed mixed states would be<sup>59</sup>

$$\Delta v_{\text{tun}}^{\nu_4} = \Delta v_{\text{tun}}^{\text{geared}} \cos^2(\chi) + \Delta v_{\text{tun}}^{\text{vdw}} \sin^2(\chi) \quad (5.3a)$$

$$\Delta v_{\text{tun}}^{\nu_5} = \Delta v_{\text{tun}}^{\text{geared}} \sin^2(\chi) + \Delta v_{\text{tun}}^{\text{vdw}} \cos^2(\chi) \quad (5.3b)$$

Here  $\chi$  is the so-called rotation angle describing the extent of mixing, and given by

$$\tan(2\chi) = 2\gamma / \Delta E \quad (5.4)$$

If we accept from 4D QM predictions<sup>36</sup> that  $\Delta v_{\text{tun}}^{\text{vdw}}$  is enhanced 2.31-fold and  $\Delta v_{\text{tun}}^{\text{geared}}$  16.6-fold from the tunneling splitting measured in  $\nu_1$ , the experimentally observed tunneling splittings can be reproduced by  $\cos^2(\chi) = 0.7$ . This would correspond to a rather significant (i.e., 30% 70%) mixing of the zero order geared bend and van der Waals stretch character in the actual  $\nu_4$  and  $\nu_5$  intermolecular modes.

We can take this analysis one step further. In the limit of strong mixing of these low frequency intermolecular degrees of freedom, one might anticipate that tunneling rates become independent of mode and depend only on total intermolecular energy and some effective 1D tunneling coordinate. This suggests that the energy dependence of the tunneling rates for the two lowest modes can be characterized by a simple 1D tunneling model and a WKB analysis of the tunneling splittings. For a 1D parabolic barrier to interconversion, the semiclassical WKB approximation predicts tunneling splittings given by:

$$\Delta\nu_{\text{tun}} = \frac{\nu_0}{\mathbf{p}} \exp\{-\beta [E^\ddagger - E_{\text{inter}}]\} \quad (5.5)$$

where  $\nu_0$  is the vibrational frequency with which the tunneling species strikes the barrier, and  $E^\ddagger$  is the height of the barrier from the zero point level (see inset in Figure 5.7). If an effective 1D model is a reasonable approximation, a plot of the tunneling splittings versus intermolecular energy should be fit by a single exponential, with the pre-factor given by  $\Delta\nu_{\text{tun}} = \nu_0/\pi \exp\{-\beta E^\ddagger\}$ , i.e., tunneling splitting observed in  $\nu_1/\nu_2$  in the absence of intermolecular excitation. Such a plot of the measured tunneling splittings is presented in Figure 5.7 indicating a remarkably good fit for both  $\nu_4$  and  $\nu_5$  excitation built on either  $\nu_1$  or  $\nu_2$ . Note that the effect of  $K$  excitation on tunneling is reasonably well represented on the same plot, which may reflect the fact that  $K$  axis excitation leads to centrifugal distortion<sup>15,56</sup> of  $(\text{HF})_2$  along the tunneling coordinate. Furthermore, the  $E^\ddagger$

extracted from this fit is  $355(2) \text{ cm}^{-1}$ , which when corrected for zero point energy in the geared bend coordinate suggests an empirical 1D tunneling barrier of approximately  $438(5) \text{ cm}^{-1}$ . This is in reasonable agreement with the initial estimates of the barrier height ( $400 \text{ cm}^{-1}$ ) in HF-stretch excited states of Pine *et al.*<sup>17</sup> From the parameters determined in the fit and the known ground state tunneling splitting, the barrier height in the ground intramolecular states is predicted to be  $366 \text{ cm}^{-1}$ , again in good agreement with the minimum energy tunneling path on the SQSBDE surface of Quack and Suhm ( $350 \text{ cm}^{-1}$ ). The key point of this analysis is that the dependence of the tunneling rate on  $\nu_4$ ,  $\nu_5$  excitation can be remarkably well represented by an effective 1D tunneling coordinate, thus corroborating the strong mixing of van der Waals stretch and geared bend degrees of freedom.

#### 5.4.4 Vibrational predissociation

Studies of vibrational predissociation in HF dimer provide information on the time scales for energy flow between high frequency (intramolecular) and dissociative (intermolecular) degrees of freedom. Previous studies of intramolecular fundamentals (i.e., with only zero point energy in the intermolecular modes), have shown that the predissociation lifetime is strongly  $\nu_1/\nu_2$  mode specific and also depends weakly on the  $K$  rotational state and

## Vibrational Predissociation Broadening in HF Dimer

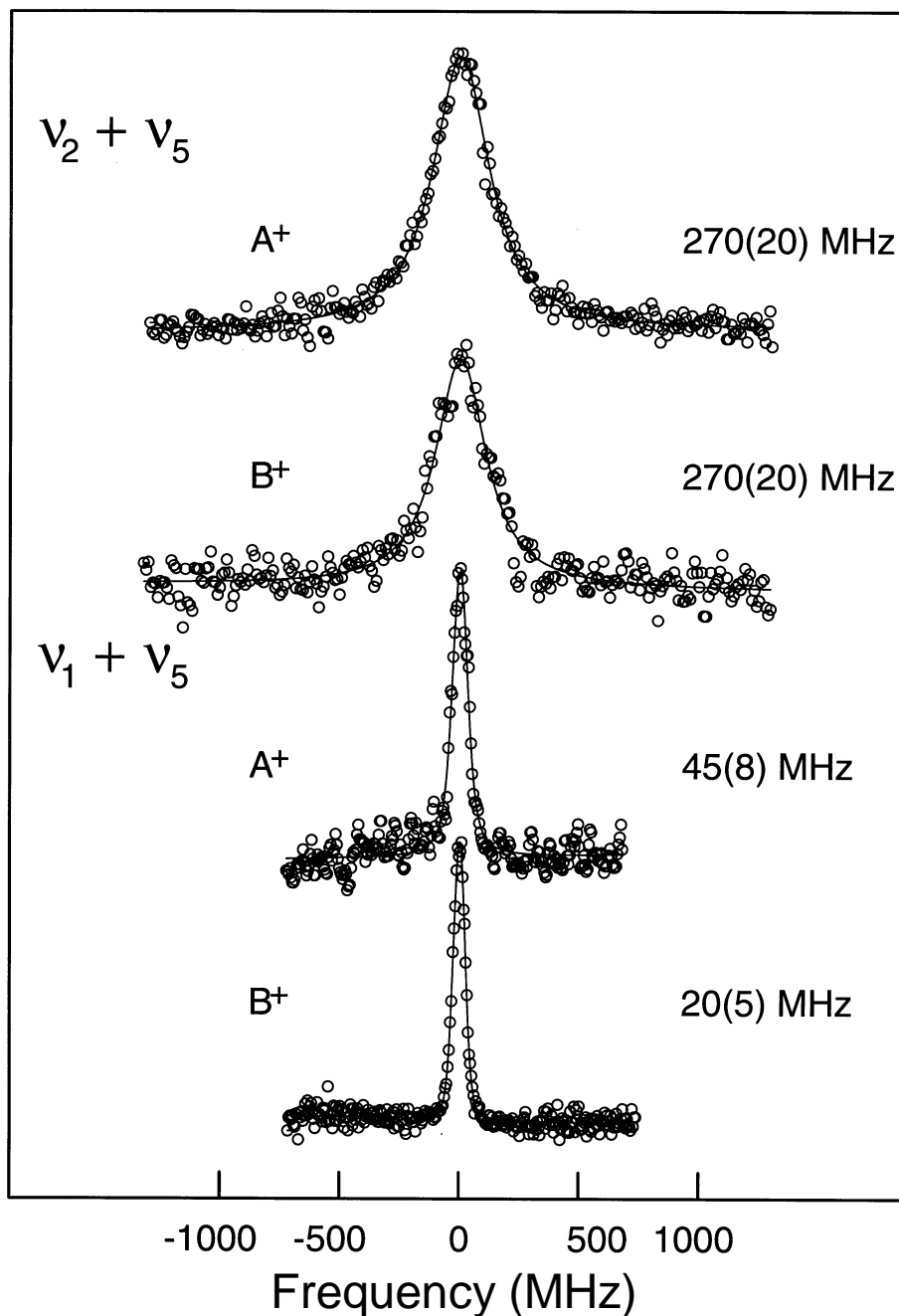


Figure 5.8 Four sample rovibrational lineshapes for the  $K=0 \leftarrow 0$  transitions of the  $\nu_2 + \nu_5$  (top) and  $\nu_1 + \nu_5$  (bottom)  $(\text{HF})_2$  combination bands. The circles represent the experimental data; the lines are the simulated Voigt profiles with homogeneous (lifetime) contributions to the broadening indicated in MHz. The mode specificity observed for the  $\nu_1/\nu_2$  intramolecular fundamentals is largely reiterated in the combination bands.

Table 5.7 Vibrational predissociation homogeneous linewidths (MHz) for HF dimer. The A<sup>+</sup> and B<sup>+</sup> symmetry labels refer to  $\Gamma_{\text{vib-tun}}$  in the upper vibrational state. The uncertainties in parentheses are in units of the last reported digit.

State	K = 0		K = 1	
	A <sup>+</sup>	B <sup>+</sup>	A <sup>+</sup>	B <sup>+</sup>
$\nu_1^{\text{a}}$	6.4(5)	9.5(5)	10.2(5)	11.8(5)
$\nu_1 + \nu_4$	25(5)	40(8)	---- <sup>b</sup>	75(50) <sup>c</sup>
$\nu_1 + \nu_5$	20(5)	45(8)		
$\nu_2^{\text{a}}$	330(30)	330(30)		
$\nu_2 + \nu_4$	---- <sup>b</sup>	300(50) <sup>c</sup>		
$\nu_2 + \nu_5$	270(20)	270(20)	400(50)	384(70)

a. Reference 15

b. not observed

c. extremely weak bands, linewidths estimated from Q-branch simulations

tunneling state probed.<sup>15</sup> In the present combination band study, we observe the  $\nu_1/\nu_2$  mode specificity to be maintained but significant effects due to initial *intermolecular* excitation are also identified.

The predissociation lifetimes are determined from a Voigt deconvolution of the HF dimer VRT lineshapes. The resulting Lorentzian component from such an analysis can be ascribed completely to predissociation broadening ( $\Delta\nu_{\text{pd}}$ ), since the factors such as pressure and power broadening are negligible for the greatly suppressed collision frequencies in a supersonic jet and typical ( $\leq 10 \mu\text{W}$ ) difference frequency power levels<sup>60</sup>. The Gaussian component for each transition arises from residual Doppler broadening in the planar expansion, and is determined

either from (i) an unconstrained least squares fit (floating both Gaussian and Lorentzian components) to selected strong transitions in the (HF)<sub>2</sub> band or (ii) by independent fits to ArHF transitions present as "impurities" in the jet for which predissociative broadening is immeasurably small.<sup>61,62</sup> High resolution scans (7.5 MHz step size, signal averaging 4-6 slit jet pulses) over transitions for several  $J$  levels in a given VRT band are fit separately. No statistically significant  $J$ -dependence is found in all the bands studied; the Lorentzian components reported in Table 5.7 therefore represent an average over all transitions observed in a given VRT band.

Even in states with *intermolecular* excitation, the predissociation rate depends predominately on the *intramolecular* mode. This is demonstrated in Figure 5.8 where typical lineshapes for transitions in the strong  $\nu_1+\nu_5$  and  $\nu_2+\nu_5$  combination bands are shown. The greater than 10-fold difference in the predissociation rates for the nearly isoenergetic  $\nu_2+\nu_5$  and  $\nu_1+\nu_5$  states is another clear demonstration of the *non-statistical* nature<sup>20</sup> of the predissociation dynamics in (HF)<sub>2</sub>. Similarly, though too weak to extract quantitative linewidth information, the linewidths for  $\nu_2+\nu_4$  excitation are definitely broader (~300 MHz) than  $\nu_1+\nu_4$  (25(5) MHz and 40(8) MHz). Thus, predissociation from  $\nu_2+\nu_4$  appears to be much *faster* than from the corresponding  $\nu_1+\nu_4$  upper states, again by roughly an order of magnitude.

Though the effect of *intermolecular* excitation on the predissociation lifetimes is less pronounced than the *intramolecular* dependence noted above, it is still quite significant. In the  $\nu_1$  supported states, where the transitions are

sufficiently narrow that small fractional changes are easier to detect, both  $\nu_4$  and  $\nu_5$  excitation results in a  $\approx 4$ -fold *increase* in the predissociation broadening. For the  $\nu_2$  supported state, the effect of  $\nu_5$  excitation is in the opposite direction, i.e.,  $\nu_2+\nu_5$  intermolecular excitation leads to a *decrease* in the predissociation rate compared with the  $\nu_2$  fundamental. These opposing trends suggest the following simple picture. In the *absence* of intermolecular excitation, the frequencies of the  $\nu_2$  and  $\nu_1$  fundamentals differ by  $62.8 \text{ cm}^{-1}$ , with corresponding predissociation rates that differ by factors of 34 to 50, for the  $A^+$  and  $B^+$  tunneling states, respectively. In the presence of intermolecular excitation, however, the two intramolecular modes are closer in energy; specifically the energy difference between the  $\nu_2+\nu_5$  and  $\nu_1+\nu_5$  origins is reduced by 20% to only  $50.7 \text{ cm}^{-1}$ . Therefore, one way to view the effect of intermolecular excitation is that it *weakens* the hydrogen bond and *decreases* the splitting between the intramolecular vibrations and thereby mixes more "donor" stretch character into the  $\nu_1$  mode and "acceptor" stretch character into the  $\nu_2$  mode, respectively. Thus,  $\nu_1$  states in the presence of intermolecular excitation mix in a small amount of  $\nu_2$  character and predissociate *more quickly*, while conversely,  $\nu_2$  states mix in  $\nu_1$  character and predissociate *more slowly*. Indeed, due to the large 34-50 fold difference in the predissociation rates of the zero order  $\nu_1$  and  $\nu_2$  states, only a relatively small (10%) amount of mixing would be necessary to produce the observed changes for the  $\nu_4, \nu_5$  combination states. This trend is also supported by spectroscopic studies of the  $\nu_6$  (out-of-plane torsion) and  $\nu_3$  (anti-gear bend) combination bands, the details of which will be presented elsewhere.<sup>63</sup>

Interestingly, the predissociation rates for  $\nu_1+\nu_4$  and  $\nu_1+\nu_5$  from a given tunneling level (i.e.,  $\Gamma_{\text{vib-tun}} = \text{B}^+$  or  $\text{A}^+$ ) are equal to within experimental uncertainty. Furthermore, even the 1.5 fractional increase in predissociation rates *between*  $\Gamma_{\text{vib-tun}} = \text{B}^+$  and  $\text{A}^+$  states in the  $\nu_1$  fundamental, is quantitatively echoed in each of the  $\nu_1+\nu_4$  and  $\nu_1+\nu_5$  combination bands. This could in principle be due to a fortuitous match between predissociative enhancement for van der Waals stretch and geared bend excitation, though this conjecture is not supported by recent Fermi Golden Rule calculations<sup>38</sup> on the QSBDE potential surface. On the other hand, these observations are consistent with the simple picture of strong state mixing between the zero order stretch-bend states, as supported by spectroscopic data throughout this discussion.

One final comment on the predissociation dynamics from combination states is in order. In previous work, Bohac and Miller<sup>21</sup> measured the state resolved photofragment distributions produced following  $\nu_1+\nu_4$  and  $\nu_1+\nu_5$  ( $K=0$ ) excitation for the  $\Gamma_{\text{tun}} = \text{A}^+$  tunneling level. The  $\nu_1+\nu_5$  excited fragments indicated a slightly hotter rotational distribution, whereas the  $\nu_1+\nu_4$  state led to higher translational recoil, i.e., qualitatively consistent with a zero order "geared bend" and "van der Waals stretch" description of the intermolecular modes. These differences in the HF fragment distributions were interpreted by the authors as evidence for *weak* stretch-bend coupling in the photodissociation dynamics. On the other hand, the weight of spectroscopic evidence discussed in this paper indicates significant mixing of "van der Waals stretch" and "geared bend" degrees of freedom in the HF-stretch excited states. The conclusions from these two

studies need not be inconsistent, however. Specifically, vibrational predissociation in  $(\text{HF})_2$  is a "rare" event, occurring on a time scale of tens of thousands of monomer vibrations.<sup>61,62</sup> Therefore from a transition state theory perspective,<sup>64</sup> the predissociation dynamics may be dominated by poor overlap of the initial wavefunction to some critical intermolecular configuration, which could be substantially different from the geometries sampled by single quantum excitation of the low frequency intermolecular modes. Indeed, this picture would be at least qualitatively consistent with the experimental observation of a relatively modest dependence of vibrational predissociation rate on intermolecular excitation. However, the coupling between angular and radial degrees of freedom could be much weaker as the inter/intramolecular coordinates approach this critical configuration, which would therefore influence the degree of state mixing inferred from a photofragment distribution.

#### 5.4.5 Comparison with 6D QM calculations

One goal of this current study is to provide spectroscopic data that will allow for a detailed evaluation of the analytical potentials constructed for  $(\text{HF})_2$ . From a variety of spectroscopic experimental quantities (i.e., rotational constants, tunneling splittings, and predissociation lifetimes), evidence has been presented that  $\nu_4$  and  $\nu_5$  access substantially mixed "van der Waals stretch" and "geared bend" zero order states. Such extensive bend-stretch state mixing, however, is not predicted from QM calculations on the SQSBDE surface. This is explicitly

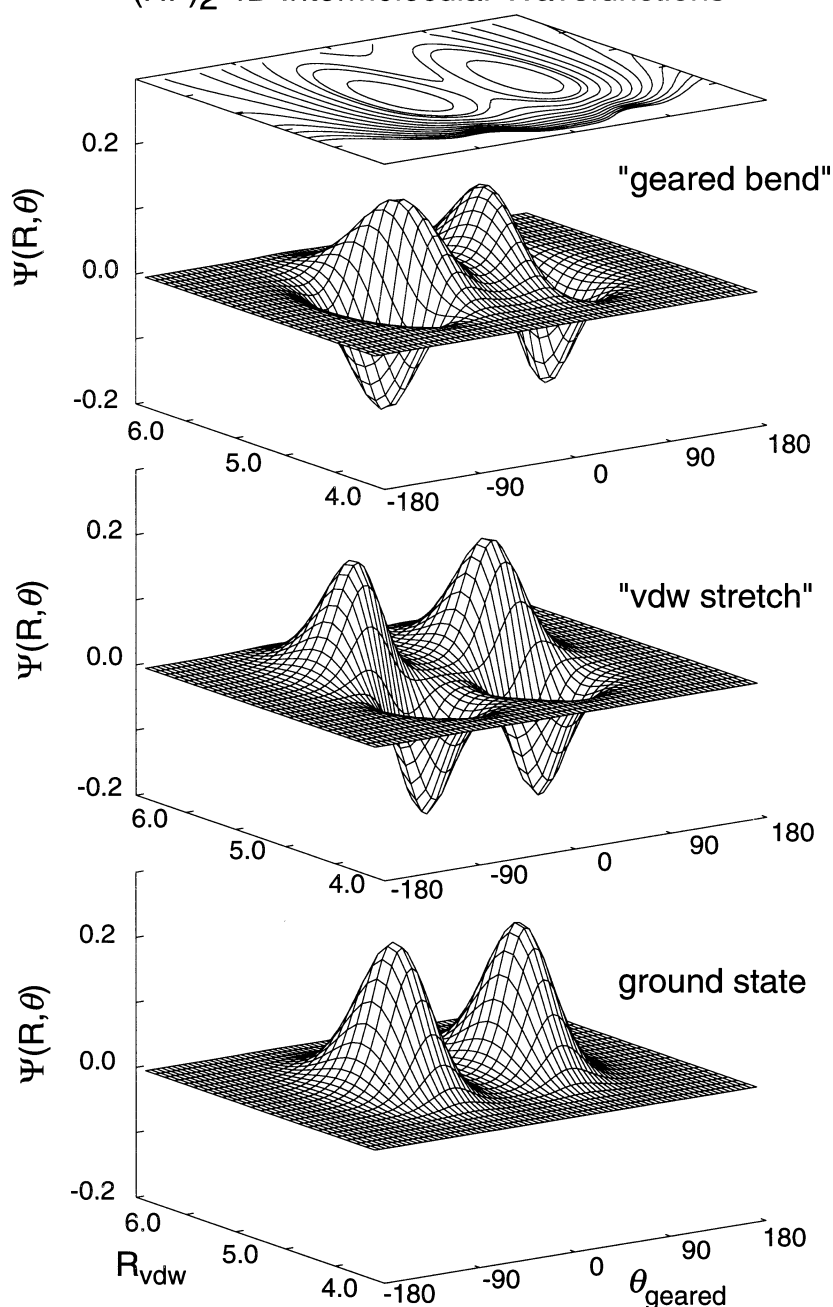
(HF)<sub>2</sub> 4D Intermolecular Wavefunctions

Figure 5.9 Wavefunctions ( $\Psi(R_{\text{vdw}}, \mathbf{q}_{\text{geared}})$ ) for the ground state of (HF)<sub>2</sub> and the first two excited intermolecular states from 4D calculations on the SQSBDE potential energy surface. Only the lower tunneling component ( $\Gamma_{\text{tun}}=A^+$ ) is shown for each state.  $R_{\text{vdw}}$  is the van der Waals stretching coordinate (Bohr) and  $\mathbf{q}_{\text{geared}}$  is a perfectly geared bending coordinate (degrees) that interconnects the two tunneling states (see text for details). A contour plot of the SQSBDE potential is included at the top of the figure; the energy contours are at equally spaced 200 cm<sup>-1</sup> intervals in the attractive part of the potential. Note the clear nodal pattern for the two excited states in the  $R_{\text{vdw}}$  and  $\mathbf{q}_{\text{geared}}$  bend coordinates, respectively. These wavefunctions are consistent with predominately decoupled angular-radial motion in these states, which is not supported by the experimental data in this paper.

demonstrated in Figure 5.9, which shows a 2D ( $R_{\text{vdw}}$ ,  $q_{\text{geared}}$ ) cut through 4D intermolecular wavefunctions calculated on the SQSBDE surface for the ground and first two excited intermolecular states (for simplicity only the *lower*  $\Gamma_{\text{tun}} = A^+$  tunneling state is shown).  $R_{\text{vdw}}$  is the radial van der Waals stretch coordinate (in Bohr), and  $q_{\text{geared}}$  is the geared bend/tunneling coordinate (in degrees) defined symmetrically around the  $C_{2h}$  transition state. For perfectly geared bending motion, the difference between  $q_1$  and  $q_2$  (the angle between either HF molecular axis and the dimer center-of-mass axis) is held fixed ( $\sim 55^\circ$ ) while the sum is varied linearly. The wavefunctions are calculated using a finite basis DVR method,<sup>65-67</sup> holding the two intramolecular coordinates fixed (at the ground vibrationally averaged value of  $1.767 a_0$ ). The calculations have been successively iterated with increasing basis set size; eigenvalues and eigenfunctions are converged to  $0.01 \text{ cm}^{-1}$  and 5% of the peak values, respectively. In the ground state eigenfunction (bottom panel), the two maxima correspond to the two tunneling configurations, FH-FH and HF-HF. It is clear from the direction of the nodal patterns that the first excited state (middle panel) is predominantly a pure "van der Waals stretch" (node @  $R_{\text{vdw}} \cong 5.3$ ) and the second excited state (upper panel) is predominantly a pure "geared bend" (node @  $q_{\text{geared}} \cong 38^\circ$ ), in contradiction with the current experimental results. Therefore, even though the calculated *eigenvalues* for  $\nu_4$  and  $\nu_5$  agree well with experiment, quantities sensitive to the *eigenfunctions* differ systematically between experiment and theory, and suggest the need for greater angular-radial coupling in the potential surface.

(HF)<sub>2</sub>  $\nu_4/\nu_5$  Intramolecular Dependence:  
Experiment and Theory

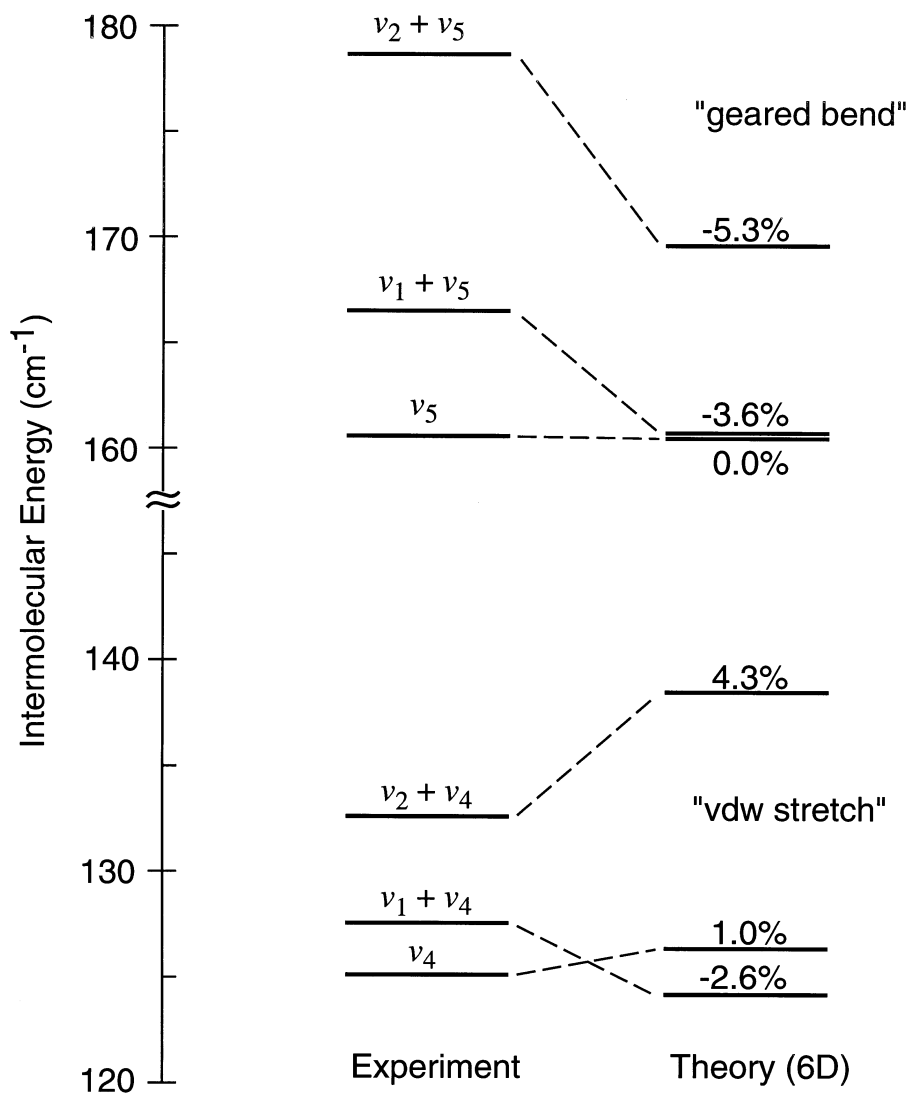


Figure 5.10 A comparison between experiment and theory for the  $\nu_4/\nu_5$  intermolecular energies in the ground and HF-stretch excited states. The theoretical frequencies are determined from 6D QM calculations (see text for details) on the SQSBDE surface. Note the considerably worse agreement between experiment and theory for the combination band versus fundamental data.

Since the current combination band data are all built on  $\nu_1/\nu_2$  intramolecular excited states, it is conceivable that these discrepancies between experiment and theory result from the influence of monomer HF-stretch excitation. Since the SQSBDE surface is a function of all 6 internal coordinates, this hypothesis can be tested by analogous 6D QM calculations in  $\nu_1/\nu_2$  vibrational states. This is computationally more difficult, since it involves calculating intermolecular "resonance" states with intermolecular plus  $\nu_1/\nu_2$  mode excitation embedded in the continuum. However, Zhang and coworkers<sup>29</sup> have recently been able to perform fully converged, 6D resonance state calculations using a finite basis DVR method for the intermolecular energies of  $\nu_4/\nu_5$  in  $\nu_1/\nu_2$  HF-stretch excited states on the SQSBDE surface. The theoretical results are plotted in Figure 5.10 along with the experimental values. The results indicate that agreement between experiment and theory for the intermolecular energies in the HF-stretch excited states is not improved; indeed, the agreement is noticeably worsened, and even the qualitative "stiffening" trends in the potential surface observed with intramolecular excitation are not consistently reproduced. Thus, it does not appear that discrepancies in experimental vs. theoretical bend-stretch state mixing can simply be explained by HF stretch excitation. On the contrary, the comparison indicates that the potential actually does a *better* job on the  $\nu_4/\nu_5$  intermolecular energies in the *ground* intramolecular state and must be refined further to reproduce both the intermolecular energies and eigenfunction properties in the excited intramolecular states. Indeed, the high resolution data presented here and in accompanying papers<sup>63,68</sup> should provide some of the detailed spectroscopic

information necessary to make an accurate 6D potential surface for (HF)<sub>2</sub> a realizable goal.

## 5.5 Summary

In this chapter, we report the measurement of new near-IR VRT spectra for (HF)<sub>2</sub> which access excited states in both the van der Waals stretching and geared bend/tunneling coordinates for excited HF-stretch vibrational states. Increases in the  $\nu_4$  and  $\nu_5$  intermolecular frequencies are quantitatively correlated with intramolecular redshift, corresponding to a "stiffening" of the hydrogen bond potential upon HF stretch excitation. This near linear correlation allows the far-IR intermolecular frequencies to be predicted from the combination band data. From a broad range of spectroscopic data presented in this paper, the  $\nu_4$  and  $\nu_5$  intermolecular states exhibit strongly coupled geared bend/van der Waals stretch motion. For example, the tunneling splittings increase approximately 10 fold with either  $\nu_4/\nu_5$  excitation, consistent with significant "geared bend" character in each of the intermolecular states. Predissociation broadening rates in the combination bands are dominated by *intramolecular* mode specificity, yet display a smaller but significant dependence on the *intermolecular* mode as well.

Full close coupled 6D QM calculations<sup>28</sup> on the SQSBDE potential<sup>24</sup> are in excellent agreement with the frequencies of  $\nu_4$  and  $\nu_5$  determined both by far-IR measurements and extrapolation of the near-IR data. However, the predicted  $\nu_4$  and  $\nu_5$  eigenfunctions are best described as a nearly decoupled van der Waals

stretch and geared bend, respectively. This is in clear contrast to the high resolution spectroscopic evidence from the present combination band data, which indicates extensive bend-stretch mixing in these low frequency modes and suggest the need for greater radial-angular coupling in the attractive well of the  $(\text{HF})_2$  potential. Measurement of both the  $\nu_3$  anti-geared bend and  $\nu_6$  out-of-plane torsion are necessary to evaluate these HF dimer potentials at even higher energies, and near-IR combination band data for these two intermolecular states will be reported elsewhere.<sup>63</sup> Also of importance in further refinement of the potential surface would be the analogous data on the intermolecular modes in the D/H substituted dimers. Toward this end, full combination band studies<sup>68</sup> of all four intermolecular modes in  $(\text{DF})_2$  (presented in Chapter 8) as well as selected intermolecular modes in DF-HF and HF-DF dimer<sup>69</sup> are presented elsewhere.

**References for Chapter 5**

- <sup>1</sup> D. J. Nesbitt, *Ann. Rev. Phys. Chem.* **45**, 367 (1994).
- <sup>2</sup> D. J. Nesbitt, *Chem. Rev.* **88**, 843 (1988).
- <sup>3</sup> R. E. Miller, *Science* **240**, 447 (1988).
- <sup>4</sup> R. E. Miller, *Acc. Chem. Res.* **23**, 10 (1990).
- <sup>5</sup> R. C. Cohen and R. J. Saykally, *Ann. Rev. Phys. Chem.* **42**, 369 (1991).
- <sup>6</sup> R. C. Cohen and R. J. Saykally, *J. Phys. Chem.* **96**, 1024 (1992).
- <sup>7</sup> T. R. Dyke, B. J. Howard, and W. Klemperer, *J. Chem. Phys.* **56**, 2442 (1971).
- <sup>8</sup> W. J. Lafferty, R. D. Suenram, and F. J. Lovas, *J. Mol. Spectrosc.* **123**, 434 (1987).
- <sup>9</sup> H. S. Gutowsky, C. Chuang, J. D. Keen, T. D. Klots, and T. Emilsson, *J. Chem. Phys.* **83**, 2070 (1985).
- <sup>10</sup> B. J. Howard, T. R. Dyke, and W. Klemperer, *J. Chem. Phys.* **81**, 5417 (1984).
- <sup>11</sup> K. von Puttkamer and M. Quack, *Chem. Phys.* **139**, 31 (1989).
- <sup>12</sup> K. von Puttkamer, M. Quack, and M. A. Suhm, *Mol. Phys.* **65**, 1025 (1988).
- <sup>13</sup> K. von Puttkamer and M. Quack, *Mol. Phys.* **62**, 1047 (1987).
- <sup>14</sup> M. Quack and M. A. Suhm, *Chem. Phys. Lett.* **171**, 517 (1990).

- 15 A. S. Pine and G. T. Fraser, *J. Chem. Phys.* **89**, 6636 (1988).
- 16 A. S. Pine and B. J. Howard, *J. Chem. Phys.* **84**, 590 (1986).
- 17 A. S. Pine, W. J. Lafferty, and B. J. Howard, *J. Chem. Phys.* **81**, 2939 (1984).
- 18 A. S. Pine and W. J. Lafferty, *J. Chem. Phys.* **78**, 2154 (1983).
- 19 R. L. Deleon and J. S. Muenter, *J. Chem. Phys.* **80**, 6092 (1984).
- 20 E. J. Bohac, M. D. Marshall, and R. E. Miller, *J. Chem. Phys.* **96**, 6681 (1992).
- 21 E. J. Bohac and R. E. Miller, *J. Chem. Phys.* **99**, 1537 (1993).
- 22 G. C. Hancock, D. G. Truhlar, and C. E. Dykstra, *J. Chem. Phys.* **88**, 1786 (1988).
- 23 P. R. Bunker, M. Kofranek, H. Lischka, and A. Karpfen, *J. Chem. Phys.* **89**, 3002 (1988).
- 24 M. Quack and M. A. Suhm, *J. Chem. Phys.* **95**, 28 (1991).
- 25 M. Kofranek, H. Lischka, and A. Karpfen, *J. Chem. Phys.* **121**, 137 (1988).
- 26 D. C. Dayton, K. W. Jucks, and R. E. Miller, *J. Chem. Phys.* **90**, 2631 (1989).
- 27 D. H. Zhang, Q. Wu, and J. Z. H. Zhang, *J. Chem. Phys.* **102**, 124 (1995).
- 28 D. H. Zhang, Q. Wu, J. Z. H. Zhang, M. von Dirke, and Z. Bacic, *J. Chem. Phys.* **102**, 2315 (1995).
- 29 Q. Wu, D. H. Zhang, and J. Z. H. Zhang, *J. Chem. Phys.* **103**, 2548 (1995).

- 30 D. H. Zhang and J. Z. H. Zhang, *J. Chem. Phys.* **98**, 5978 (1993).
- 31 M. Quack and M. A. Suhm, *Chem. Phys. Lett.* **234**, 71 (1995).
- 32 W. C. Necochea and D. G. Truhlar, *Chem. Phys. Lett.* **231**, 125 (1994).
- 33 W. C. Necochea and D. G. Truhlar, *Chem. Phys. Lett.* **224**, 297 (1994).
- 34 J. K. Gregory and D. C. Clary, *Chem. Phys. Lett.* **237**, 39 (1995).
- 35 P. Jensen, P. R. Bunker, A. Karpfen, M. Kofranek, and H. Lischka, *J. Chem. Phys.* **93**, 6266 (1990).
- 36 D. H. Zhang and J. Z. H. Zhang, *J. Chem. Phys.* **99**, 6624 (1993).
- 37 D. H. Zhang and J. Z. H. Zhang, *J. Chem. Phys.* **98**, 5978 (1993).
- 38 D. H. Zhang, Q. Wu, J. Z. H. Zhang, M. von Dirke, and Z. Bacic, *J. Chem. Phys.* **102**, 2315 (1995).
- 39 A. S. Pine, in *Structure and Dynamics of Weakly bound Molecular Complexes*, edited by A. Weber (D. Reidel Publishing Company, New York, 1987), pp. 93.
- 40 E. Riedle, S. H. Ashworth, J. T. Farrell, Jr., and D. J. Nesbitt, *Rev. Sci. Instrum.* **65**, 42 (1994).
- 41 J. T. Farrell, Jr., S. Davis, and D. J. Nesbitt, *J. Chem. Phys.* **103**, 2395 (1995).
- 42 A. S. Pine, *J. Opt. Soc. Am.* **64**, 1683 (1974).
- 43 G. Guelachvili, *Opt. Comm.* **19**, 150 (1976).
- 44 C. M. Lovejoy and D. J. Nesbitt, *J. Chem. Phys.* **87**, 1450 (1987).

- 45 C. Amiot and G. Guelachvili, *J. Mol. Spectrosc.* **51**, 475 (1974).
- 46 P. R. Bunker, *Molecular Symmetry and Spectroscopy* (Academic Press, 1979).
- 47 H. C. Longuet-Higgins, *Mol. Phys.* **6**, 445 (1963).
- 48 M. Quack, *Mol. Phys.* **34**, 477 (1977).
- 49 J. T. Hougen and N. Ohashi, *J. Mol. Spectrosc.* **109**, 134 (1985).
- 50 I. M. Mills, *J. Chem. Phys.* **88**, 532 (1984).
- 51 M. A. Suhm, J. T. Farrell, Jr., A. McIlroy, and D. J. Nesbitt, *J. Chem. Phys.* **97**, 5341 (1992).
- 52 M. Quack and M. A. Suhm, *Chem. Phys. Lett.* **183**, 187 (1991).
- 53 C. M. Lovejoy and D. J. Nesbitt, *J. Chem. Phys.* **91**, 2790 (1989).
- 54 M. D. Marshall, P. Jensen, and P. R. Bunker, *Chem. Phys. Lett.* **176**, 255 (1991).
- 55 S. C. Althorpe, D. C. Clary, and P. R. Bunker, *Chem. Phys. Lett.* **187**, 345 (1991).
- 56 P. R. Bunker, T. Carrington, Jr., P. C. Gomez, M. D. Marshall, M. Kofranek, H. Lischka, and A. Karpen, *J. Chem. Phys.* **91**, 5154 (1989).
- 57 G. C. Hancock and D. G. Truhlar, *J. Chem. Phys.* **90**, 3498 (1989).
- 58 H. Sun and R. O. Watts, *J. Chem. Phys.* **92**, 603 (1990).
- 59 M. D. Schuder, C. M. Lovejoy, R. Lascola, and D. J. Nesbitt, *J. Chem. Phys.* **99**, 4346 (1993).

- 60 C. M. Lovejoy and D. J. Nesbitt, *J. Chem. Phys.* **86**, 3151 (1987).
- 61 G. T. Fraser and A. S. Pine, *J. Chem. Phys.* **91**, 3319 (1989).
- 62 P. A. Block and R. E. Miller, *Chem. Phys. Lett.* **226**, 317 (1994).
- 63 D. T. Anderson, S. Davis, and D. J. Nesbitt, *J. Chem. Phys.* **105**, 4448  
(1996)
- 64 R. Schinke, *Photodissociation Dynamics* (Press Syndicate of the University  
of Cambridge, Cambridge, 1993).
- 65 Z. Bacic and J. C. Light, *J. Chem. Phys.* **85**, 4594 (1986).
- 66 Z. Bacic and J. C. Light, *J. Chem. Phys.* **86**, 3065 (1987).
- 67 Z. Bacic and J. C. Light, *Ann. Rev. Phys. Chem.* **40**, 469 (1989).
- 68 S. Davis, D. T. Anderson, and D. J. Nesbitt, *J. Chem. Phys.* **105**, 6645  
(1996)
- 69 J. T. Farrell, Jr., M. A. Suhm, and D. J. Nesbitt, *J. Chem. Phys.* **105**, 9313  
(1996)